Chapter 8
Triggering and Synchronization of Stick-Slip: Experiments on Spring-Slider System

T. Chelidze, T. Matcharashvili, O. Lursmanashvili, N. Varamashvili, N. Zhukova, and E. Meparidze

8.1 Introduction

Triggering and synchronization are the two faces of the same coin; both effects imply that the additional forcing causing triggering and synchronization is much smaller than the main driving force, which means that these phenomena are connected with nonlinear interactions of objects, namely, with initiation of instability in systems that are close to the critical state. In a seismic process, the main driving component is the tectonic stress; earthquakes are considered as dynamic instabilities generated in the process of friction (stick-slip) between faces of geological faults (Brace and Byerlee, 1966; Kanamori and Brodsky, 2004; Ben-Zion, 2008). The additional forcing is exerted by various external impacts: tides, reservoir exploitation, big explosions, magnetic storms, etc.

Experimentally, triggering is revealed by correlation of some single external impact and single seismic event with some delay; according to this definition, statistics of triggering events is relatively small. Synchronization, on the other hand, is defined as "the adjustment of rhythms due to an interaction" and this means that it manifests itself not in rear solitary acts but in systematic multiple process, which provides relatively rich statistics and allows applying rigorous methods of assessment of the strength of synchronization.

We can illustrate the essence of synchronization phenomenon by considering the relaxation or integrate-and-fire oscillator under periodic forcing (Fig. 8.1).

T. Chelidze (✉), T. Matcharashvili, O. Lursmanashvili, N. Varamashvili, N. Zhukova, and E. Meparidze
M. Nodia Institute of Geophysics, 1 Alexidze str., 0171 Tbilisi, Georgia
e-mail: tamaz.chelidze@gmail.com

V. de Rubeis et al. (eds.), *Synchronization and Triggering: from Fracture to Earthquake Processes*, GeoPlanet: Earth and Planetary Sciences 1,
DOI 10.1007/978-3-642-12300-9_8,

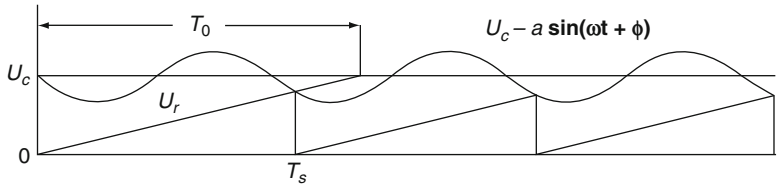

Fig. 8.1 Scheme of synchronization of relaxation oscillator by periodic forcing: T_0 is the period of non modified relaxation process and T_s is the same for a synchronized one, U_r is the current value of the voltage, U_c is the critical value of voltage for discharge of non synchronized generator and U_c is the same for a synchronized one

The examples are numerous, from biology to electricity and mechanics. Such oscillator exhibits interchange of the epochs of slow evolution, when accumulation of energy U_r takes place and the rapid phase, when, on reaching some critical threshold U_c, a fast discharge of accumulated energy occurs. The application of periodic forcing $a(\sin \omega t + \phi)$ affects the process, as now the critical threshold is $U_c + a(\sin \omega t + \phi)$. Accordingly, it changes the natural frequency T_0 of relaxation oscillator to some other value T_s, which now becomes a characteristic (synchronized) frequency of system.

8.2 Electromagnetic Triggering of Slip

Up to now, the problem of triggering and synchronization of seismic process is far from being resolved and relevant publications are controversial due to the complexity of natural processes (Beeler and Lockner, 2003; Scholz, 2003a; Grasso, 1998; Nikolaev A, 1994; Nikolaev V, 2003; Scholz, 2003; Kanamori and Brodsky, 2004; Ben-Zion, 2008). Understanding of main regularities can be obtained in controllable experiments. We carried out laboratory experiments on the slider-spring system with superimposed pulse or periodic electromagnetic (EM) forcing, which is weak in comparison with the main dragging force of the spring. The use of EM impact was prompted by experiments carried out in 1983-1988 by the Institute of High Temperatures of Russian Academy of Sciences (IHT RAS) at the Bishkek test area in Central Asia. After performing series of MHD soundings as well as "cold" discharges, initially aimed at finding resisitivity precursors of strong earthquakes in upper layers of the Earth crust, an unexpected effect of micro-seismicity activation by strong EM pulses has been discovered (Tarasov et al., 1999). We reproduced the effect in laboratory conditions and it turns out that EM forcing is a flexible tool for the study of triggering and synchronization phenomena in laboratory slider experiments (Chelidze et al., 2002; Chelidze and Lursmanashvili, 2003; Chelidze, Matcharashvili, 2003; Chelidze et al., 2005; Chelidze et al., 2006; Chelidze et al., 2007; Chelidze et al., 2008, Chelidze et al., 2009).

8.2.1 EM Triggering – Experimental Setup

The experimental setup has been designed in such a manner that the mechanical system could be easily driven to the critical state where the triggering of mechanical instability by some weak impact, such as electrical pulse, becomes more probable. The system (Fig. 8.2) consists of two pieces of rock; the upper piece can slip on the fixed supporting sample if a special frame tilts the latter one up to the critical angle α_c.

The electrical part consists of EM pulse generator and acoustic signals amplifier. The signal from the standard generator of 0.5–5 V amplitude is applied to the input of the amplifier and goes out from the output with the amplitude up to 1300 V. Up to 10 DC-pulses of this amplitude were applied to the sample. The duration of pulses was from 5 to 10 s; interval between pulses was also from 5 to 10 s. The high voltage source (discharger) was also used. Another amplifier was designed for registration of acoustic signals from the sensors which respond to the slip events. The amplifier's output voltage was sufficient for registration of acoustic signals by the sound card of PC. The scanning of the process was performed on the frequency 96 kHz, i.e., the sampling rate was 1/96 000 s.

Electrodes were applied in the following ways: (i) to the bottom of the supporting sample in a coplanar manner or to the sides of the supporting sample (the first mode); (ii) to the upper surface of the sliding sample and the bottom of the supporting one (the second mode). In the first case, the EM field is oriented roughly parallel to the slip surface and in the last case current lines are normal to it. In most cases, the supporting and the slipping blocks were prepared from basalt; these samples were saw-cut and roughly finished. The slipping block is 10 cm long, 10 cm wide and 2 cm thick. Other samples, such as granite, labradorite, and glass, which were better finished, were also tested. The height of surface protuberances was in the range of 0.1–0.2 mm for basalt samples and 0.05–0.1 mm for other ones.

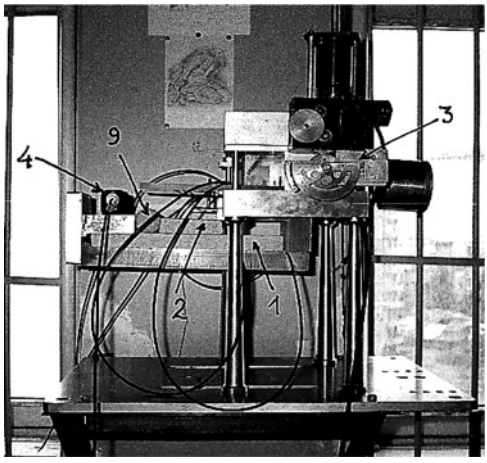

Fig. 8.2 Mechanical setup for slip initiation on the inclined surface: 1 – supporting (fixed) sample; 2 – slipping sample; 3 – slope regulating unit; 4 – acoustic emission sensor; 9 – shock absorber

The basalt samples were preferred because they do not contain significant quantity of piezoelectric minerals.

8.2.2 EM Triggering Experiments

The main objective of experiments was to find out whether EM-pulse could indeed displace the rock sample resting on the supporting sample at the slope of support, less than but close to the critical slip angle. The details of experiments are presented in (Chelidze et al., 2002; Chelidze et al., 2004).

Slip events were registered as acoustic bursts (Akay, 2002) by the sound card of PC.

It should be noted that although high voltage was applied to the outer surfaces of samples, the voltage in the gap between sliding surfaces was much less, of the order of 1 V.

8.2.3 Experimental Procedure and Case Stories

After finding the critical angle (Fig. 8.3), the slope of support was decreased by 0.1–2°. In this state, the upper sample was stable for many hours (2 days), which means that other sources of instability, such as building vibration by trucks, elevator, wind, etc, were not strong enough to initiate the slip. The critical angle for the rough surface varies from one test to another because it is impossible to reproduce exactly the arrangement of asperities between the support and the

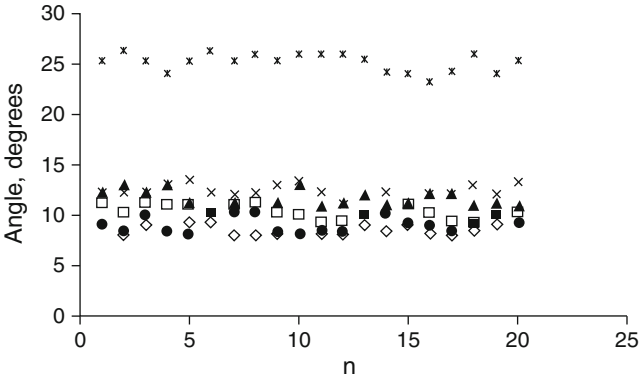

Fig. 8.3 The critical angle of slip (degrees) for various samples on the same supporting material versus number of experiment n. * – basalt, x – glass cylinder (diameter 14 cm, thickness 12 mm), □ – glass cylinder (diameter 7.5 cm, thickness 10 mm), ◇ – glass cylinder (diameter 2 cm, thickness 10 mm).

slipping blocks in different experiments. The scatter in values of critical angle for the same sample is of the order of $\pm 2.5^\circ$ so we can define only the average value of α_c (Fig. 8.3), which changes from one test to another. Because of the critical angle scatter, before the EM impact the sample was kept at the angle less than the (average) critical one for 10 minutes, and only after this exposure it was subjected to the EM-impacts also for 10 minutes.

That allows assessing correctly the statistics of EM-activation, as the probability of slip in the time intervals without EM-impact can be compared with that in the time intervals covering the whole EM-activation period. The activation period lasts several minutes and it includes also the gaps between pulses. A sequence of pulses applied in a single experiment and gaps between them will be related as a run. Practically the probability of slip without EM-impact at $\alpha < \alpha_c$ was zero: no slip was observed during any of 10 min. preliminary repose periods (500 min in total).

8.2.4 EM Triggering — The First Mode

We found that the application of EM-pulses in the first mode, i.e., to the coplanar electrodes at the bottom of support, initiates slip in approximately 40 cases from 600 runs (i.e., the slip initiation probability is around 0.07) either during pulse (i.e., in the active phase), or after it (i.e., in the passive phase). The last observation means that the polarization of the sample can be important for the slip initiation. As the delay of slip after switching off the pulse sometimes was considerable (seconds), our guess is that in this case polarization is related mainly to the accumulation of the bulk charge near electrode surfaces. This phenomenon (electrode polarization) is well known; it accompanies the application of high voltage to ionic conductors and its relaxation is slow.

A typical recording of acoustic emission generated by the slip event is shown in Fig. 8.4a and b for different time scales.

Besides the pulse generator, a second source of high voltage, namely the electrical discharger TESLA OPOCMO TVI 200, has been used for initiation of slip. In this case, the voltage applied was of the order of 10 kV. Again series of pulses were applied to the sample in the first mode and in this case the probability of slip initiation was much higher – around 0.2.

8.2.5 EM Triggering — The Second Mode

In the second mode, the electrodes were applied to the upper facet of the slipping block and to the bottom side of support, i.e., in this case the applied electrical field was oriented in the direction normal to the slip surface.

That means that when the EM is applied in the second mode, it increases the friction force (EM field hampers the slip) according to electrostriction rule (Tamm, 1956).

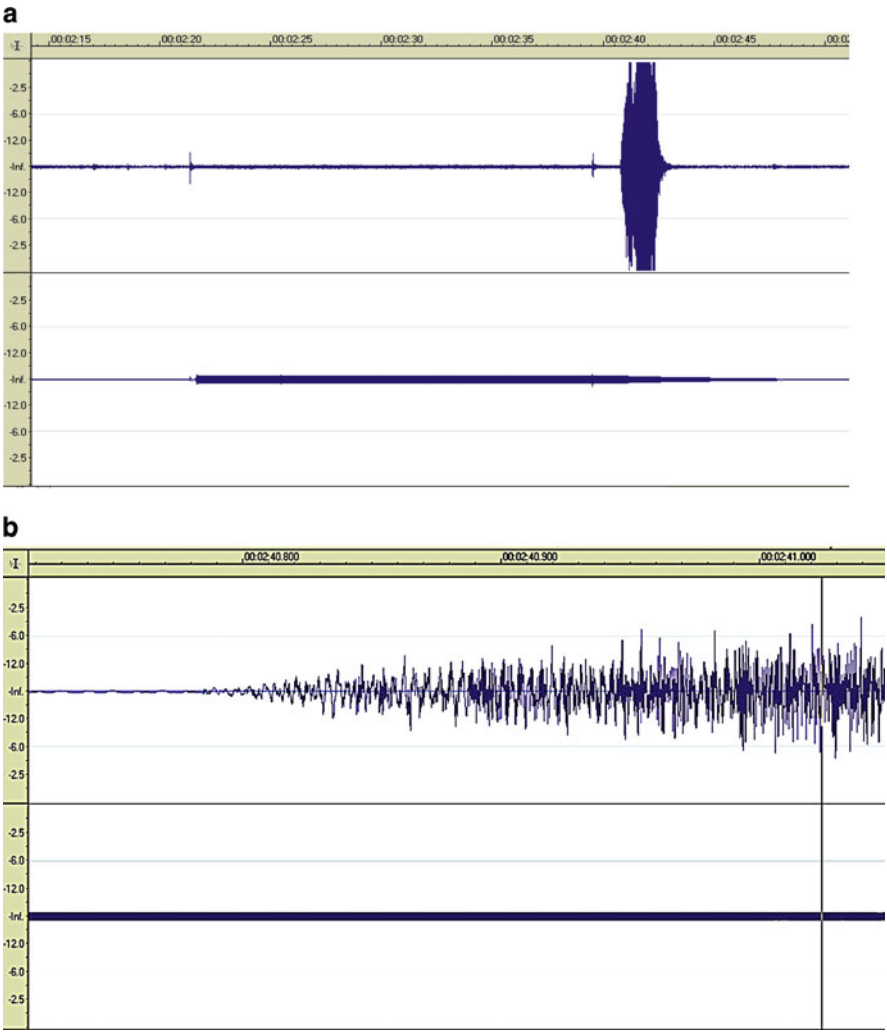

Fig. 8.4 (**a**) Recording of acoustic emission generated by the electromagnetically initiated slip of the basalt sample (upper trace). Lower trace shows EM pulse switching on (thick line) and switching off (thin line) periods. The slip was initiated just after the active period. y-axis shows amplitude of the signal in db, x is the time axis. (**b**) The initial part of the same recording with the stretched time axis

8.2.6 Finding Mechanical Equivalent of EM Impact

For assessment of mechanical equivalent of electrical impact, both direct and theoretical methods were used.

In the first case, the mechanical force initiating slip at the same angle $\alpha < \alpha_c$ that has been set in experiments with EM-impact, was measured by spring and torsion dynamometers (accuracy of ± 0.01 N and ± 0.005 N, respectively). Both methods gave comparable results. The force, equivalent to slip-initiating EM-impact, is of the order of 0.2 N. Another way to get mechanical equivalent is to calculate it from the general equation of balance of forces for a sample placed on the inclined plane:

$$F = mg(\mu \cos \alpha - \sin \alpha) \tag{8.1}$$

As long as μ is known (for basalt samples $\mu = 0.47$), slip-initiating force can be calculated for any angle. For example, if α_c equals 25°, at $\alpha = 24°50'$ the initiating force is 0.42 N. This value is of the same order as in direct experiments (0.2 N).

Thus, in the situation close to the critical one, even 0.2 N force can initiate the slip of a sample weighting 700 g.

Our guess is that the EM impact is equivalent to the above value, i.e., it promotes slip in the first mode and hampers it in the second mode by the additional force of the order of 0.2–0.4 N.

8.3 Analysis of Recorded Acoustic Waveforms

The results of experiments, namely, acoustic signals emitted during initiated slip, were recorded as *.wav files with 96 kHz sampling frequency at 8 bit resolution. The 3D patterns of original signals were obtained using program WaveLab (Figs. 8.6a, 8.7a in Chelidze et al., 2004). They show that some periodic components span the whole time axis. As they are present even before slip initiation, we guess that they are connected with weak vibrations due to computer and generator fans and other alias sources.

For filtering the background noise and further analysis of recordings, *.wav files were imported to the MatLab and their wavelet transform was performed. Mayer wavelet with a compact support in the frequency domain was used. Calculated wavelet coefficients were used for filtering of original signal. Namely, the wavelet components related to frequency range of noise, quite different from these of slip movement, were excluded. The de-noised signal reproduces the slip-generated wave package quite satisfactorily. Resulted de-noised data were analysed again using Wavelab, and filtered 3D images of frequency distribution in the time domain during slip were obtained (Figs. 8.6b and 8.7b in Chelidze et al., 2004b).

The consideration of the above images shows that the emitted signals are concentrated in 500–20,000 Hz frequency range and the manner of slip initiation (EM or mechanical) does not change significantly the wavelet and spectral patterns.

8.4 The Elementary Theory of EM Coupling with the Friction Force

In order to understand physics of EM-slip it is necessary to consider fundamentals of surface phenomena. Intermolecular and intersurface forces, responsible for adhesion and friction, can be loosely divided into three categories: (i) purely electrostatic, arising from the Coulomb interaction between charges; (ii) polarization forces arising from the dipole moments, induced by internal (bound charges, dipoles) or external electric field; (iii) quantum-mechanical forces, responsible for covalent bonding and steric interactions. All these forces can act simultaneously, resulting in some total adhesion (friction) force. For friction we have:

$$F_f = \mu F_n, \tag{8.2}$$

where μ the is friction coefficient and F_n is the normal component of force acting on the body (gravity, compression).

From the above classification it can be deduced that in principle as far as intersurface forces are of electromagnetic origin, external electrical field can affect the adhesion (friction) forces, changing μ and thus initiating slip of the body placed on the inclined plane. We can rewrite (8.2) in the following way:

$$F_f = \mu(F_n + F_p), \tag{8.3}$$

where μ is the friction coefficient and F_p is the increment (decrement) of normal component of force due to the application of EM field.

Of course, coupling of EM-impact with friction in a sample containing piezoelectric materials is a trivial phenomenon. However, the EM-activation of slip is clearly observed on samples that are practically free of piezoelectric minerals (basalts). That is why we exclude the piezoelectric effect as a principal mechanism of EM-slip.

The elementary theoretical model of EM coupling with friction can be formulated in the following way. It is well known that the application of EM field to a dielectric invokes some forces acting upon molecules of the body; the resultant force is called the electrostriction force F_p which is affecting the whole sample. The force is proportional to the gradient of the field intensity squared and it carries away the sample in the direction of the largest intensity. The tension tensor $\vec{T}_n$ operating on the element of dielectric's surface in EM field of intensity E on the assumption that the sample of dielectric constant ε is surrounded by the immobile dielectric medium in *ESU* system is (Tamm, 1956):

$$\vec{T}_{np} = \pm \frac{\varepsilon + \frac{\partial \varepsilon}{\partial \delta}\delta}{8\pi} E^2 \vec{n}, \tag{8.4}$$

where the sign (+) applies when the field $\vec{E}$ is parallel to the external normal $\vec{n}$ to the considered surface element, and the sign (−) when the field $\vec{E}$ is normal to $\vec{n}$.

We can imagine that the elastic strings are stretched along field lines (Tamm, 1956): in our case, they pull together the surfaces of sliding and supporting samples in the second mode or build the side thrust on each other according to (8.4). The latter case corresponds to the first mode and the former one to the second mode of EM-triggering.

The above equations can be simplified if the dielectric increment due to the striction force is negligible: $(\partial\varepsilon/\partial\delta \to 0)$. Introducing the area of dielectric's surface S and taking into account the above assumption, the electrostriction force is:

$$\vec{F}_p = \pm\frac{\varepsilon}{8\pi}E^2\vec{n} = \pm\frac{\varepsilon S}{8\pi}\left(\frac{\Delta V}{d}\right)^2\vec{n} \tag{8.5}$$

where ΔV is the applied voltage and d is the distance between electrodes; the sign depends on the mutual orientation of dielectric's surface and electrical field.

Substituting into (8.5) the values: $\Delta V = 1200$ Volt $= 4$ ESU, $\varepsilon = 5$; $S = 100$ cm^2 and $d = 5$ cm, which correspond to the capacitor, created by two electrodes we obtain:

$$\left|\vec{F}_p\right| = 0.5 \text{ dyne} = 5\ 10^{-6}\text{N}$$

That is much less than the experimental values of electromagnetic pull force, which is of order of 0.2 N. Here we have to note that the value of $(\Delta V/d)$, substituted in (8.5), is an average value for the whole system and on the contact between two blocks the gradient can be quite different. The matter is that the most part of the voltage drop occurs in the gap and the local gradient of EM field in the gap between samples can be much larger than for the whole system between electrodes. In order to assess the forces acting in the narrow gap between slipping and supporting samples, it is necessary to consider the gradient in the gap between the samples. The inner surfaces of slipping and supporting samples carry bound charges, due to the polarization of material, and thus create the local gradient of electrical field in the gap. The opening of the gap itself is varying; we can introduce some effective value of opening d_{eff}. Then, applying again the equation (8.6) to the "inner" capacitor, we obtain the electrostriction force F_{pi} acting on the gap surfaces as follows:

$$\vec{F}_{pi} = \pm\frac{\varepsilon_{eff} S}{8\pi}\left(\frac{\Delta V_{eff}}{d_{eff}}\right)^2\vec{n}, \tag{8.6}$$

where $\Delta V_{eff}/d_{eff}$ is the effective voltage gradient in the gap and ε_{eff} is the effective dielectric constant of the gap, which is between values of ε for the air and the sample: $1 < \varepsilon < 5$.

Assuming $\varepsilon_{eff} = 2.5$, $S = 100$ cm^2, we have to put in equation (8.6) the gradient $(\Delta V_{eff}/d_{eff)}) = 0.07$ V/cm in order to obtain the experimental values of slip-initiating electrostriction force, namely, $F_p \approx 0.2$ *N*.

Thus the expression (8.7) can be written, taking into account (8.6):

$$F_f = \mu\left(F_n + F_{pi}\right), \tag{8.7}$$

which is similar to the expression for the friction force, taking into account the pore pressure term (Sibson, 1994).

The above value of F_{pi} can be considered as an order of magnitude of electrostriction force that promotes the slip in the first mode and hampers it in the second mode, according to the expression (8.6) for the accepted set of parameters.

Both our experiments and theoretical considerations are related to the "dry" environment, namely, to the 60 ± 20% humidity of the atmosphere at a temperature of (20 ± 5)°C.

It is interesting to note that somehow similar effect of synchronization of acoustic vibrations (not stick-slip motion) in rock samples by the superimposed EM forcing has been observed by Chernyak (1978).

In the "humid" environment, when the rock's pore space is fully or partially saturated with water, additional factors should be taken into account: (i) the pore pressure increment (decrement) in the gaps, caused by the electrokinetic flow of fluid at the application of EM field; (ii) the change of surface fracture energy of cracks due to electroosmotic fluid inflow into the cracks of an undersaturated rocks due to the EM impact. Both these factors can facilitate fracture process in water-bearing rocks.

8.5 Synchronization of Stick-slip

8.5.1 Synchronization: Experimental Setup

Experimental setup in synchronization experiments represents a system of two horizontally oriented plates of roughly finished basalt (Fig. 8.5). A constant pulling force F_p of the order of 10 N was applied to the upper (sliding) plate; in addition, the same plate was subjected to periodic mechanical or electric perturbations with variable frequency and amplitude (from 0 to 1000 V), which was much weaker (of order of 1 N) compared to the pulling force; the electric field was normal to the sliding plane. Acoustic bursts accompanying slip events were registered by the sound card of PC. Details of the setup and technique are given in (Chelidze and Lursmanashvili, 2003).

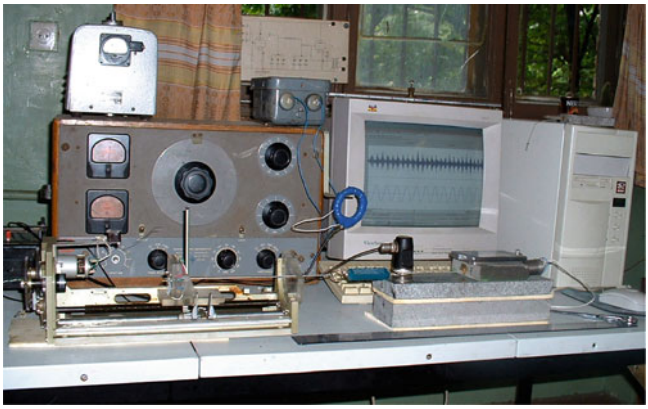

Fig. 8.5 Laboratory setup for synchronization experiments

8.5.2 Signal Processing: Separation of AE Wave Trains

The first step of AE data analysis consists in signal conditioning and wave trains separation. A relatively simple form of signal conditioning is calculation of its envelope by the Hilbert transform (Kurz et al., 2004). The Hilbert transform generating phase shift of $\pi/2$ is defined as:

$$\hat{R} = \frac{1}{\pi} \int_{-\infty}^{\infty} \frac{R(t)}{\omega - u} du = H\{R(t)\} \tag{8.8}$$

It is a causal transfer function which behaves like a filter of a real time dependent function *R(t)*.

Then the envelope time function *E(t)* can be calculated:

$$E(t) = \sqrt{R(t)^2 + \hat{R}(t)^2} \tag{8.9}$$

Squared and normalized envelope of the signal leads to suppression of noise of lower amplitude and to increase of the signal content of higher amplitude (Fig. 8.6).

Then, the envelope can be used to estimate the onset of the signal or for correct signal detection in general. Strictly speaking, in order to determine the onset time of AE signal, AIC (Akaike Information Criterion) function was calculated according to Maeda (1985). The minima of AIC function correspond to AE signal onsets; afterwards, the onsets can be correlated with forcing signal phase (Fig. 8.7).

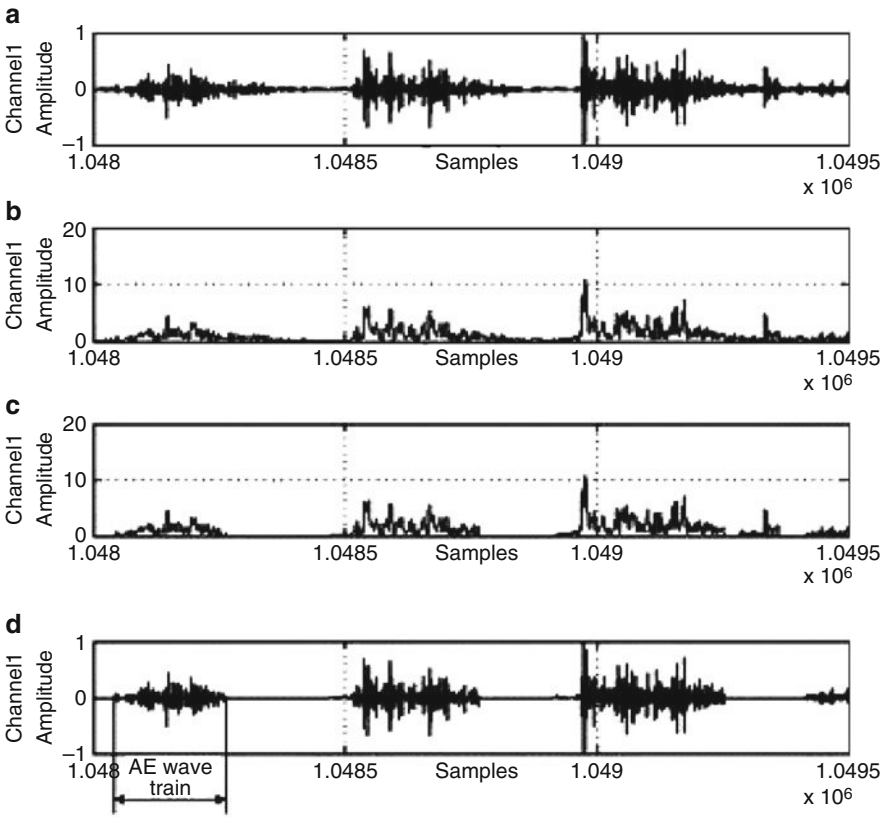

Fig. 8.6 Processing of the acoustic signal: (**a**) source (initial) signal; (**b**) Hilbert transform of the source signal; (**c**) filtered Hilbert-transformed signal using Standard Deviation criterion – only the part of signal of amplitude less than 3σ was eliminated; (**d**) the recording (a) filtered from the noise according to criterion (c)

Typical examples of filtered AE recordings during various regimes of stick-slip are presented in Fig. 8.8. The random sequence of AE, obtained for stiff springs, probably corresponds to macroscopically "stable" sliding, and quasi periodic sequences – to macroscopically "instable" process, characteristic for soft springs.

After such a processing, the catalogue of waiting times of acoustic bursts has been compiled.

Besides, the catalogue of "magnitudes" of AE was also compiled. The energy released by acoustic pulse (or the power of AE) was calculated as the plot area delineated by a singled acoustic burst recording.

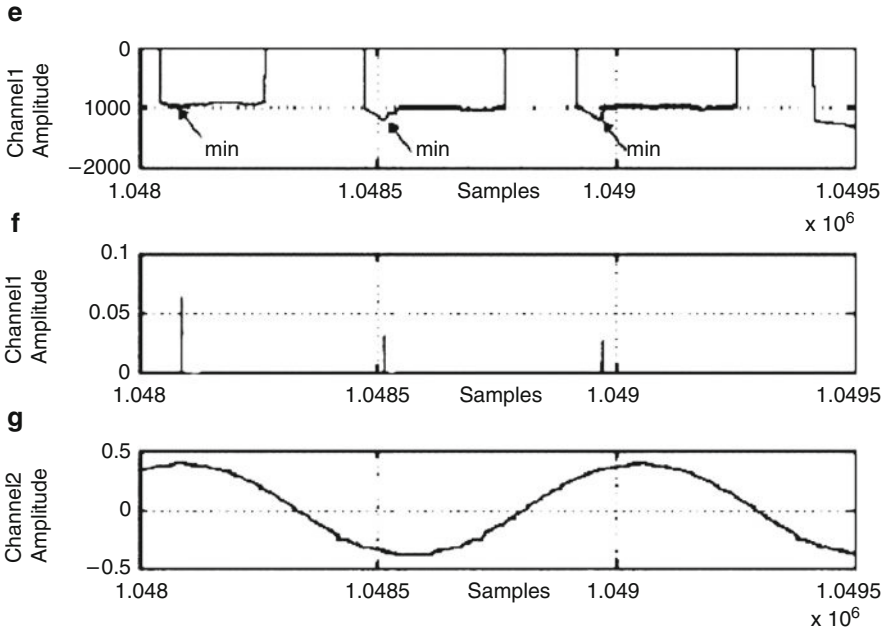

Fig. 8.7 The AIC (Akaike Information Criterion) function of AE signal: (**e**) the minima of AIC function are picked; (**f**) corresponding AE signal onsets are located; (**g**) onsets can be correlated with forcing signal phase

8.5.3 Synchronization: Results

In our experiments the following parameters were varied: (i) the stiffness of the spring, K_s; (ii) the frequency, f, of superimposed periodical perturbation; (iii) the amplitude of the excitation (applied voltage V_a); (iv) the direction of applied electrical field; (v) the velocity of drag, v_d; vi) the normal (nominal) stress σ_n.

The typical background behavior of the system with stiff spring during conventional stick-slip is presented in Fig. 8.9a. It is evident that in these conditions AE events do not manifest any visible periodicity at the time scale from several to hundred milliseconds. In case of soft spring, the friction movement is realized by quasi periodic slips (Fig. 8.9b).

Slip with superimposed periodic low-frequency EM field ($f \approx 60$ Hz) of varying intensity, oriented normally to the slip surface, is presented in Figs. 8.10a, b, c. The significant synchronization at this frequency occurs at $V_a \geq 500$ V. Under EM excitation the AE events (micro slips) occur twice per period (Fig. 8.10c). The maxima of AE coincide (approximately) with the extreme points of oscillation.

Synchronization was observed only at some definite values of the set of parameters (K_s, f, V_a). The "phase diagram" for variables f and V_a, or the so-called Arnold's tongue (see Pikovsky et al., 2003) is presented in Fig. 8.11.

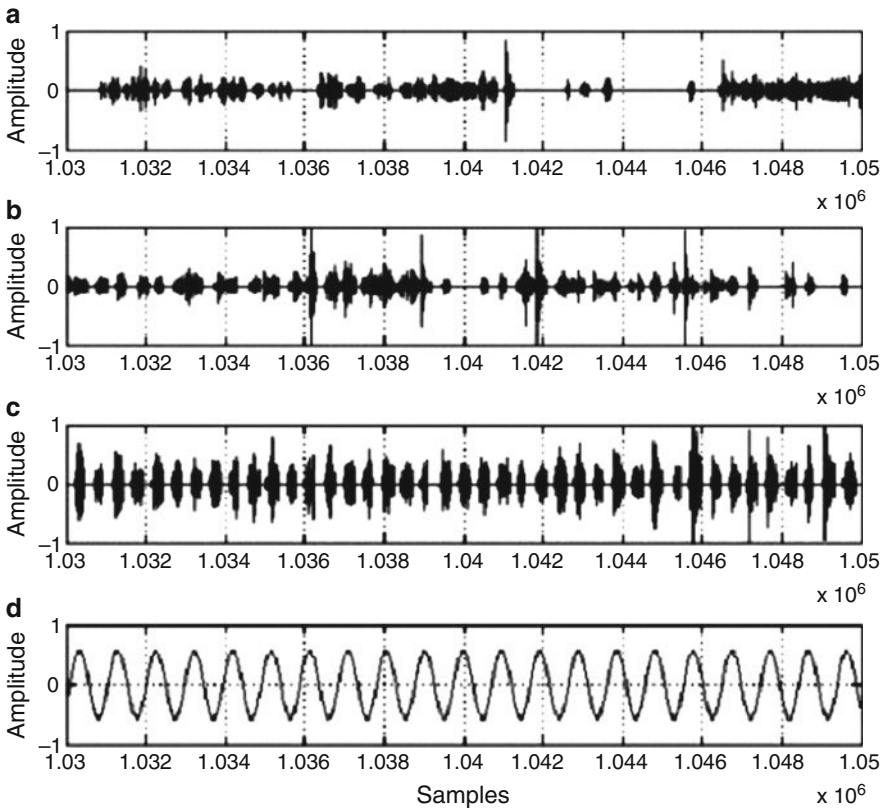

Fig. 8.8 Filtered AE recordings for various regimes of stick-slip: (**a**) and (**b**) – stiff springs; (**c**) – soft spring; (**d**) – forcing signal

It should be noted that the phenomenon of synchronization was observed only with the EM field directed normally to the slip surface. When the EM field was applied to the vertical sides of the slipping block, that is, roughly parallel to the slip plane, we were not able to observe the effect of synchronization. We conclude that the synchronization is related to "electromagnetic braking" of slip at passing the extreme values of sinusoidal EM forcing and a sudden slip after the accumulation of enough stress provided by spring pull.

Moistening of the slip surface by wetted blotting paper does not affect the "mechanical' synchronization, but practically kills the "electromagnetic" synchronization.

We observe transition (bifurcation) in stick-slip from 1:2 or period doubling synchronization, when two slip events occur per a period of EM forcing, to 1:1 synchronization, when one slip event occur per a period of forcing (Fig. 8.12) at simultaneous action of direct $V(0)$ and periodic $V(p)$ voltages; transition occur at $V(0) > V(p)$.

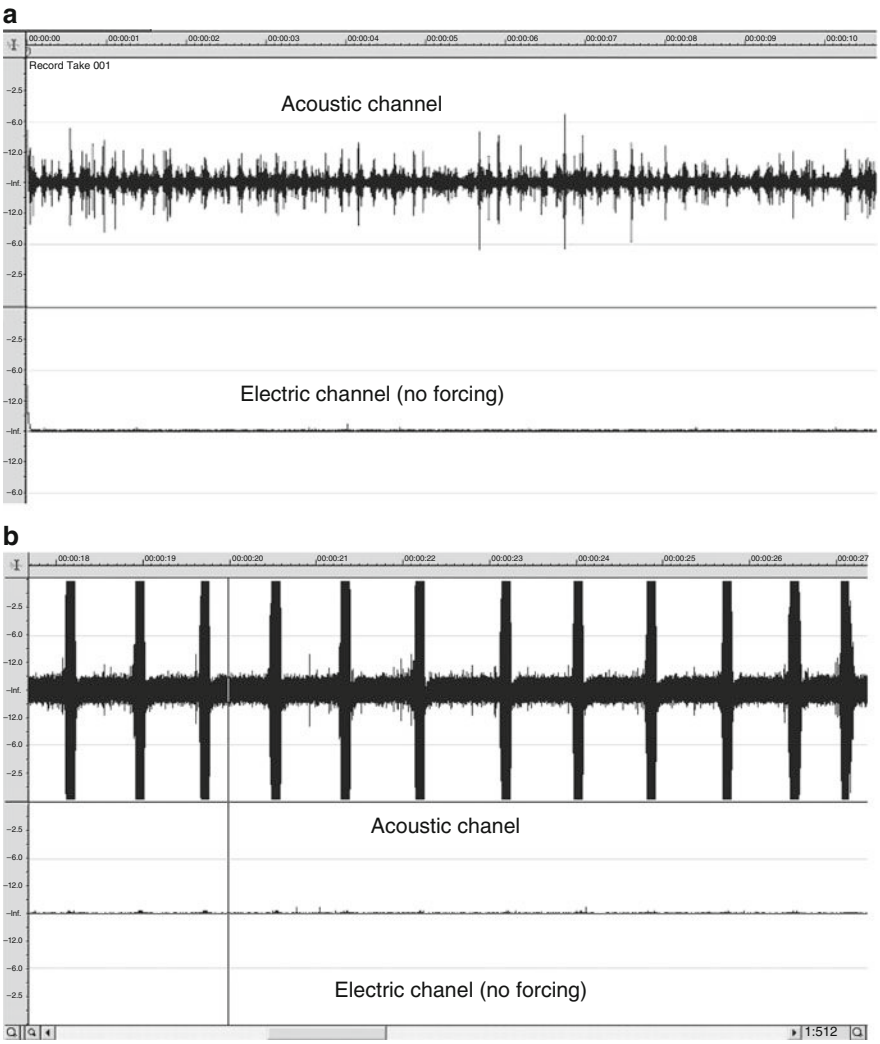

Fig. 8.9 Typical acoustic emission during slip without periodical impact: (**a**) stiff spring; practically random release of acoustic bursts. The stiffness of spring $K_s = 1000$ N/m; $\sigma_n = 2$ kPa.; the mean drag velocity $v_d = 2.5$ mm/s; dragging force $F_d = 3.5$ N; T = 20°C; humidity W = 40%; (**b**) soft spring; quasi periodic acoustic bursts (without external periodical forcing) with the mean waiting time 0.7 sec during natural slip; $v_d = 1.45$ mm/s; $F_d = 3$ N; $K_s = 125$ N/m; T = 20°C; W = 50%. Here and in Figs. 8.10a, b, c; 8.12; 8.15a, b; 8.26; 8.27a; 8.28a; 8.29a; and 8.30a, b, the amplitude of AE and synchronizing field is given in dB

Synchronization affects not only waiting times, but also the frequency-energy distribution: the amplitudes of bursts are much less scattered than in the absence of periodic forcing.

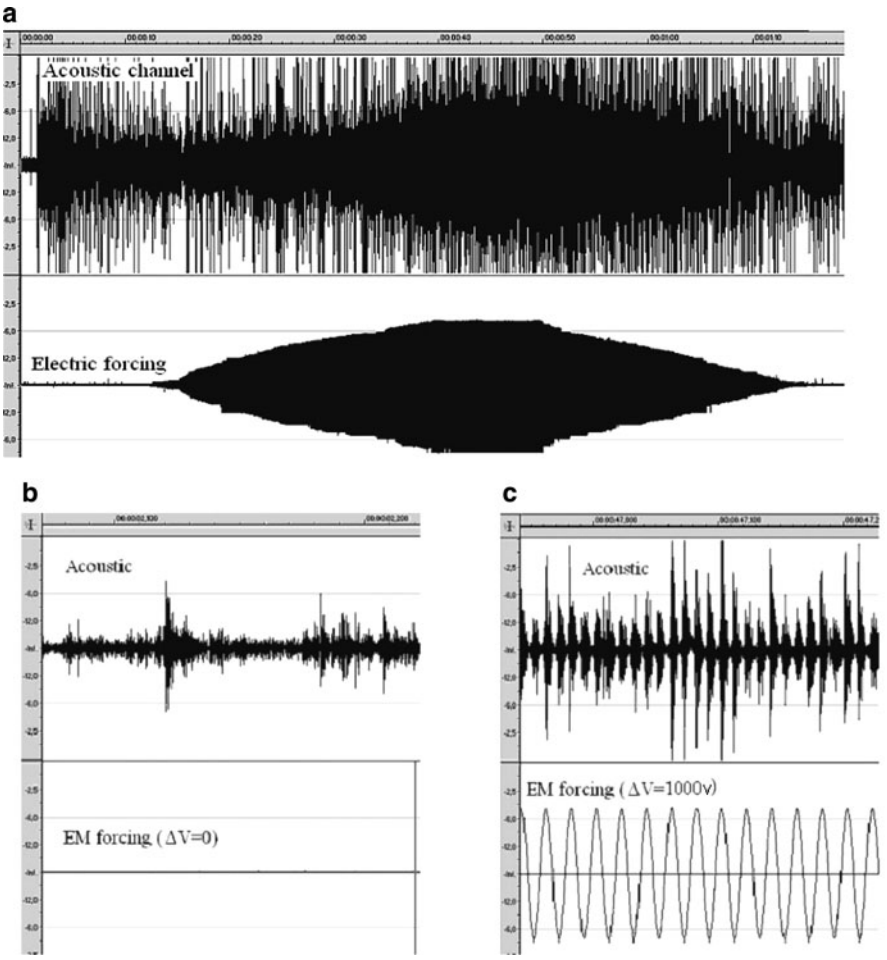

Fig. 8.10 (**a**) Acoustic emission during slip under periodical external voltage varying from zero to 1000 V; (**b**) the extended part of record with zero EM forcing; (**c**) the extended middle part of record under maximal EM forcing. Note complete phase synchronization – PS

We tried to plot (Fig. 8.13) the slopes of distribution of number of AE events versus reduced power of AE (that is, an analogue of Gutenberg-Richter plot) in sequential windows (time intervals) using data of experiment with different intensity of forcing (see Fig. 8.10 a).

The (negative) slope of the plot is maximal in the most synchronized part of AE record on Fig. 8.10a, due to increasing contribution from small events leading to appearance of plateau in the small energy section and decreasing of number of strong events (see Fig. 8.11 in Chelidze et al., 2005). This means that the energy is pumped from large events to some intermediate scale ones. As the contribution from very large events is limited, the plot in this interval looks like

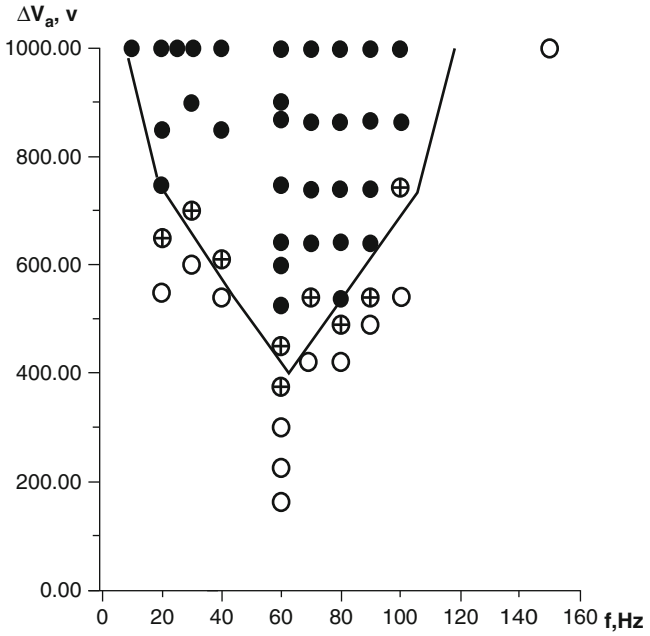

Fig. 8.11 Stick-slip synchronization area (Arnold's tongue) for various intensities (V_a) and frequencies (f) of the external EM forcing. Filled circles – perfect, circles with crosses – intermittent, and empty circles – absence of synchronization

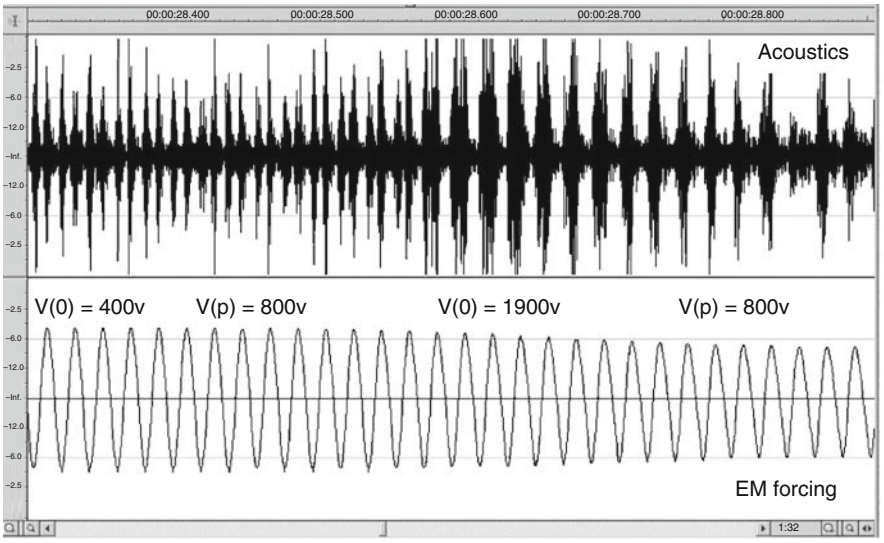

Fig. 8.12 Transition (bifurcation) in stick-slip from 1:2 synchronization (period doubling) to 1:1 synchronization at simultaneous action of direct V(0) and periodic V(p) voltages; transition occurs at $V(0) > V(p)$

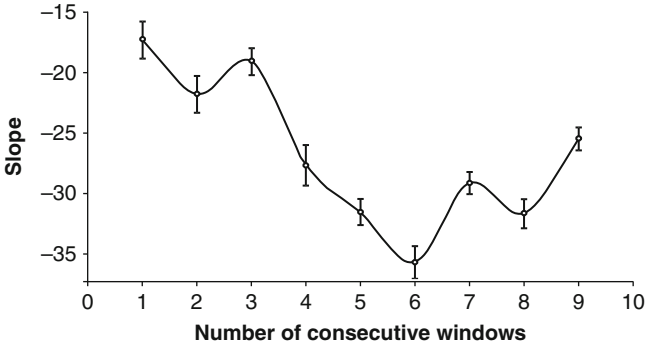

Fig. 8.13 Slopes of linear parts of magnitude-frequency (log cumulative value of number of AE events versus reduced power of acoustic emission) plots versus the serial number of 300 data-length sliding windows in the time series of AE. The data of experiment with different intensity of forcing (Fig. 8.10a) were used. The (negative) slope of the plot is maximal in the most synchronized part of AE record (Fig. 8.10c), due to increasing contribution from small events leading to appearance of plateau in the small energy section and decreasing number of strong events (Fig. 8.11 in Chelidze et al., 2005). The middle part of analyzed time series (window 6) was the most synchronized one

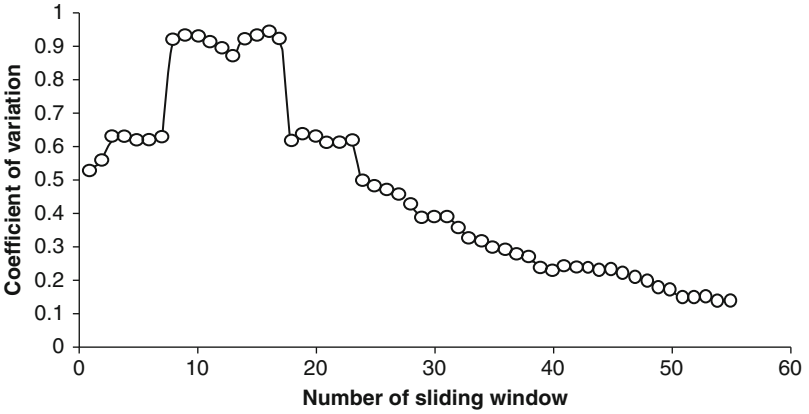

Fig. 8.14 Coefficient of variation of power of acoustic emission time series at increased external forcing for 500 data length sliding window with 50 data shift. Here only half of record (Fig. 8.10a) is used from the start of test to the maximal synchronization state

magnitude-frequency distribution for characteristic earthquake model; hence, the distribution of energies becomes less scattered due to increasing share of "characteristic" events.

A decrease of contribution of extreme events at synchronization is confirmed by calculation of the coefficient of variation CV (CV = standard deviation/mean). As shown in Fig. 8.14, the extent of the deviation from the mean value of released AE power calculated for consecutive sliding windows decreases at synchronization.

This means that synchronization limits the energy release associated with individual events (quantization effect). Sudden decrease or total cessation of synchronizing forcing is followed by acoustic burst of much larger energy than during the periodic forcing (Fig. 8.15a, b).

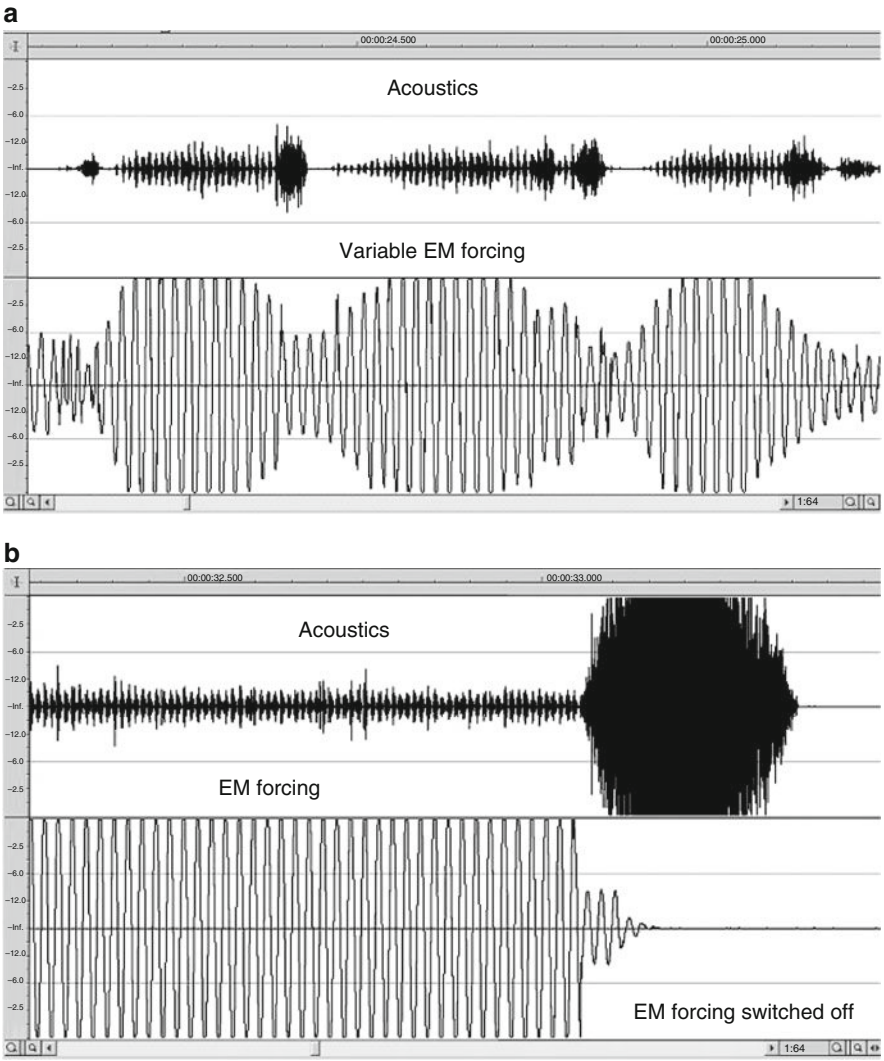

Fig. 8.15 Increased acoustic energy release after decreasing (**a**) or total cessation (**b**) of periodic EM forcing, which means that synchronization limits the energy release associated with a single event (quantization effect)

8.6 Synchronization: Quantitative Analysis

Several tools for quantitative analysis of the strength of synchronization (Ditto, 1990; Zbilut, 1992; Rosenblum et al., 1996; Rosenblum et al., 1998; Kantz, 1997; Quiroga et al., 2002; Pikovsky et al., 2003; see also Chapter 1) were tested on the recordings of stick-slip process, where the superimposed periodic EM field intensity was raised monotonously from zero to 1000 V and then decreased in the same way to zero (Fig. 8.10a).

In order to assess synchronization in the qualitative manner we used the easiest approach for estimating phases of acoustic signal: digitized waveforms were transformed to sharp spikes to have well pronounced markers. Then time series (catalogues) of time intervals between consecutive maximums (waiting times) ($\Delta t = t_i - t_{i-1}$) in wave trains for π periods of external sinusoid (Fig. 8.10c) were composed (the time scale in Figs. 8.16 – 8.20 corresponds to sequential values of t_i).

In order to achieve more reliable phase construction and precise synchronization testing, various tools of nonlinear dynamics (synchronization) theory described in Chapter 1 were applied to experimental data obtained under variable intensity of forcing; the results are shown in Figs. 8.13–8.14 and 8.16–8.20. All these approaches yield similar results.

In Fig. 8.17 we present the temporal evolution of phase difference $\Delta\phi$ obtained from Hilbert transform of waiting times time series. Well-defined horizontal part of $\Delta\phi$ versus t (Fig. 8.17) represents the time during which the acoustic emission becomes phase synchronized to the external sinusoidal forcing in the wide range of their amplitudes (from approximately 500 V to 1000 V). Clear phase synchronization is especially obvious in Fig. 8.17, as long as in the most synchronized part of the plot the phase difference variation $\Delta\phi$ does not exceed 10 radian (compare with the total increment $\Delta\phi$ of 1800 radian during the whole experiment).

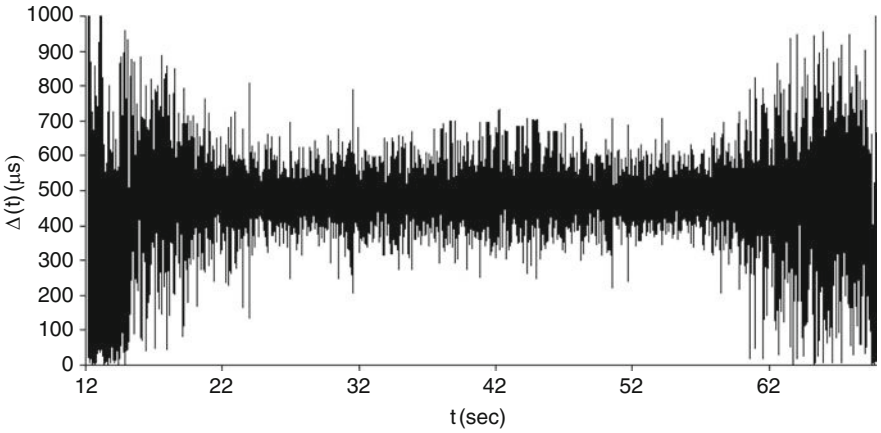

Fig. 8.16 Time series of waiting times between consecutive maximal amplitudes of acoustic signals in consecutive π-periods of external forcing for a whole record (compare with Fig. 8.10a)

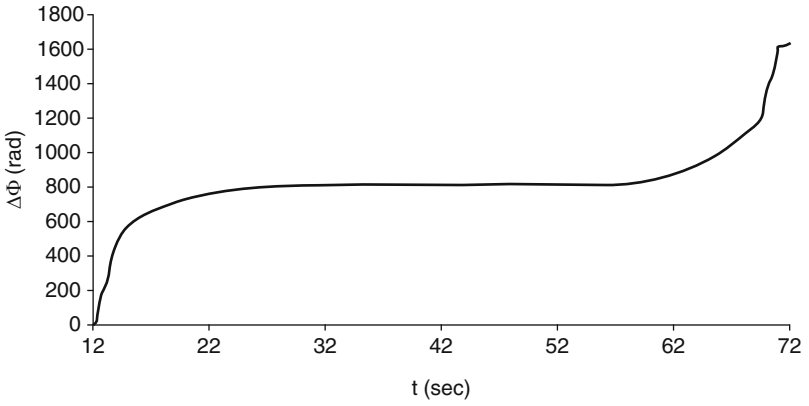

Fig. 8.17 Phase difference $\Delta\Phi$ between the sequence of maximums of acoustic emissions' bursts (AE catalogue) and external sinusoidal forcing for the whole record (Fig. 8.10a)

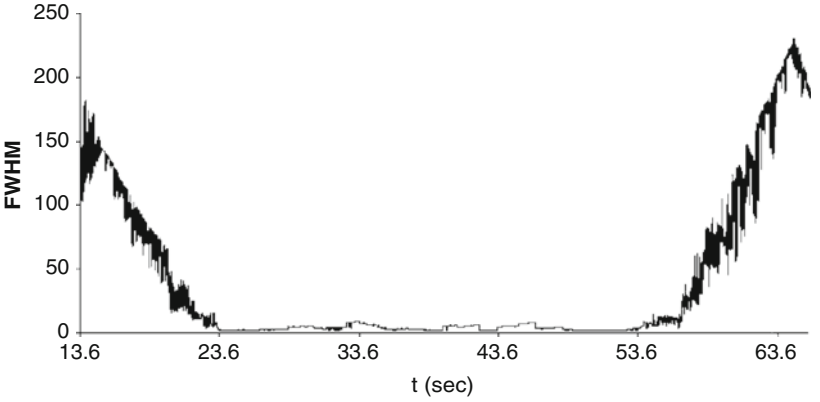

Fig. 8.18 Variation of the full width of probability density distribution of phase differences between the catalogue of acoustic events and periodic signal at a half maximum (FWHM), calculated for consecutive sliding windows, containing 500 events

It is known that the probability density distribution must be narrower for the synchronized signal compared to a non-synchronized one. As follows from Fig. 8.18, the full width at half maximum (FWHM) of probability density distribution of phase differences between AE pulses and sinusoidal forcing is indeed much narrower for the synchronized part of Fig. 8.10a.

Frequency locking, expressed as a minimum of the phase diffusion coefficient, is also a quantitative measure of the phase synchronization (see Fig. 8.19).

Moreover, clear decrease of Shannon entropy value S indicates that dynamics of acoustic emission becomes much more regular in the synchronized part of acoustic emission data set (Fig. 8.20).

One of interesting methods of revealing synchronization in relaxation-type processes is a "gap" technique (Lursmanashvili, 2001), which is described in detail

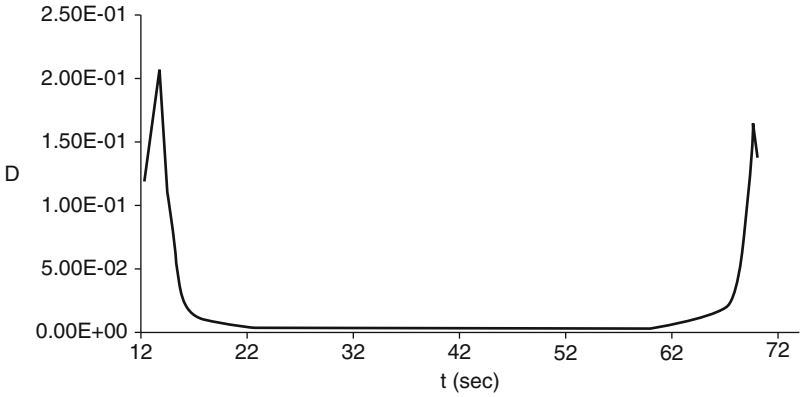

Fig. 8.19 Variation of phase diffusion coefficient *D* of phase differences, calculated for consecutive sliding windows, containing 500 events

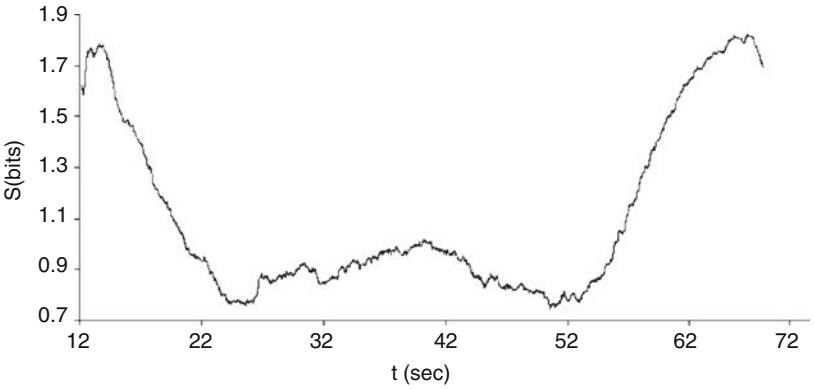

Fig. 8.20 Variation of Shannon entropy *S* of phase differences, calculated for consecutive sliding windows, containing 500 events

in Chapter 18 and which has an analogue in the analysis of radio technical systems (Blekhman, 1988). It is founded on the effect of concentration of slips (and associated seismic/acoustic events) in the definite phases of forcing period. Of course, this means that the occurrence of dynamic events in the remaining phases of forcing is less probable (prohibited). The width of the prohibited zone is larger for stronger synchronization. Of course, some intervals of silence can occur just randomly, but these intervals are relatively short and are distributed randomly relative to the forcing phase. These short gaps can be considered as a noise; the gaps due to synchronization are much wider. The method has been tested on the laboratory spring-slider model with mechanical forcing.

Consider stick-slip as a nearly periodic relaxation process, where the stress is accumulated for a long time in order to release it in a fast slip. As this last phase is very short, the duration of a whole cycle is practically equal to that of accumulation stage.

Assume that a periodic relaxation process with period τ is exposed to also periodic forcing of period T. Let us suppose that the forcing period is not known exactly, but some preliminary guess on the range of periods can be made. Is it possible to retrieve the unknown forcing period accurately from the observed modified relaxation process? So, the objective is to find exact forcing period from a given sequence of onsets of slips $d(j), j = 1,2,3, \ldots . m$. Here m is the total number of slips. We are looking for the forcing period inside the interval $[T_{min}; T_{max}]$ of a width $\Delta T = T_{max} - T_{min}$. We use a scanning window with the optimal length dT, which is much less than ΔT. The window length dT is calculated by the following empirical formula:

$$dT = T^2 min/50t, \tag{8.10}$$

where t is the duration of experiment. As a result we will have $n = \Delta T/\, dT$ (virtual) periods to test inside the chosen interval of periods ΔT. For the $T(i)$-th trial (virtual) forcing period we have:

$$T(i) = T_{min} + i \times\, dT, \quad i = 0, 1, 2, 3.....n \tag{8.11}$$

For revealing phase synchronization the times of slip occurrences $d(j)$ are divided by the corresponding period $T(i)$:

$$\mathrm{d(j)}/T(i); \quad j = 1, 2, 3... ....\mathrm{m}; \; i = 1, 2, 3... ....n. \tag{8.12}$$

Let us consider for each period $T(i)$ the remainder of the above division $F(j,i)$:

$$F(j, i) = remainder(d(j)/T(i)) \quad j = 1, 2, 3.....m; \quad i = 1, 2, 3.....n.$$

For revealing phase synchronization just the non integer part is essential as it characterizes the distribution of phases of "discharges" inside the trial forcing period. For convenience these values are normalized in the following way:

$$F^n(j, i) = F(j, i)T(i) \times 1000 \tag{8.13}$$

After such a normalization, the considered values of $F_n(j,i)$ do not depend on the absolute value of trial period $T(i)$ and are distributed inside the range [0;1000]. The normalized phases are arranged according to their ascending values and the largest free-of-slips interval between neighboring phases or the local maximal "gap" width $dF(j, i)^{loc}_{\max}$ is found for each trial period $T(i)$. As a result, two numerical sequences for $T(i)$ and $dF(j, i)^{loc}_{\max}$ are obtained. The graph of $dF(j, i)^{loc}_{\max}$ versus $T(i)$ actually forms a spectrum of local maxima of gaps widths for a chosen range of trial forcing

periods. The largest gap (or the absolute maximum in the set of local ones) returns the value of the sought forcing period.

The method has been tested on the laboratory spring-slider model with mechanical forcing. The results are shown in Figs. 8.21–8.23.

In these experiments the forcing frequency (30 Hz) was known beforehand and the objective was to retrieve it from the observed data as if it were unknown. So the known forcing frequency was used only for validation of the gap method. The amplitude of mechanical forcing was changed (namely, the excitation of mechanical vibrator was realized by application of voltages of 4, 5 and 6 V

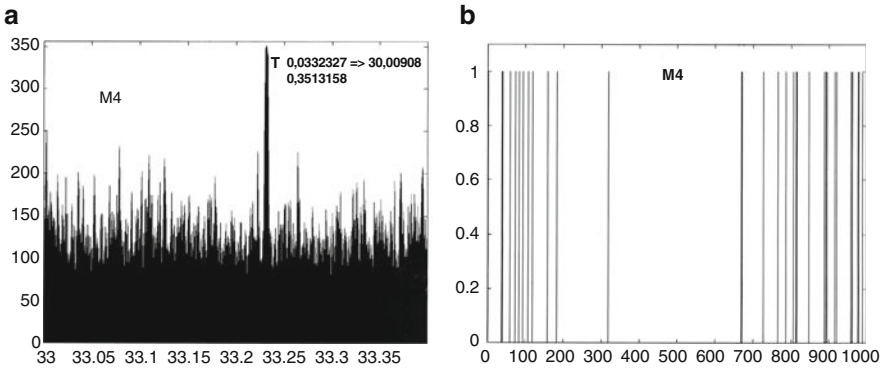

Fig. 8.21 (**a**) Recurrence spectrum of local maxima of gaps widths for a chosen range of trial forcing periods spectrum of slips for exciting voltage of 4 V: *Y*-axis — the local maxima of the gap widths $dF(j,i)^{loc}_{\max}$; *X*-axis — trial periods $T_i \cdot 1000$; (**b**) The distribution of slip moments inside the genuine forcing period T_{ig} divided in 1000 intervals

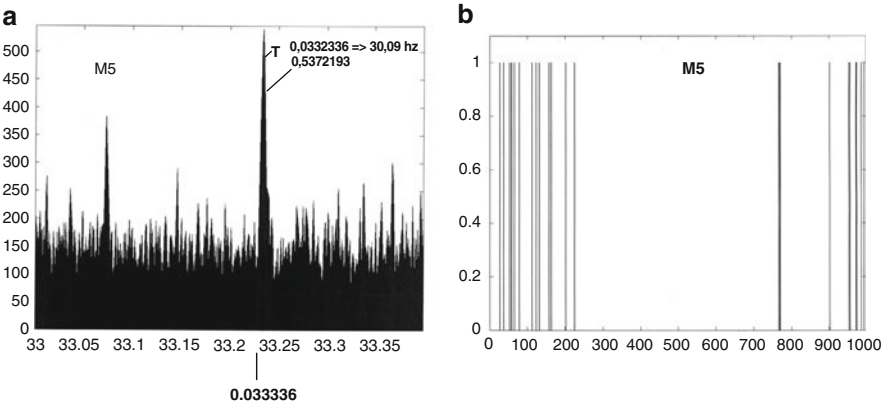

Fig. 8.22 (**a**) Recurrence spectrum of local maxima of gaps widths for a chosen range of trial forcing periods spectrum of slips for exciting voltage of 5 V: *Y*-axis – the local maxima of the gap widths $dF(j,i)^{loc}_{\max}$; *X*-axis – trial periods $T_i \cdot 1000$; (**b**) The distribution of slip moments inside the genuine forcing period T_{ig} divided in 1000 intervals

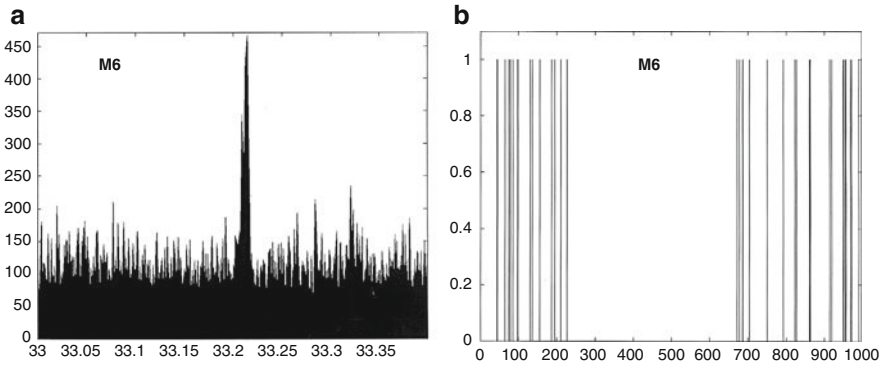

Fig. 8.23 (**a**) Recurrence spectrum of local maxima of gaps widths for a chosen range of trial forcing periods spectrum of slips for exciting voltage 6 V: *Y*-axis — the local maxima of the gap widths $dF(j,i)^{loc}_{\max}$; *X*-axis — trial periods $T_i \cdot 1000$; (**b**) The distribution of slip moments inside the genuine forcing period T_{ig} divided in 1000 intervals

respectively, in Figs. 8.21–8.23). Figs. 8.21a, 8.22a, 8.23a show the hidden periodicity of slips (in particular, recurrence spectra of local maxima $dF(j,i)^{loc}_{\max}$ for each trial period T_i) and Figs. 8.21b, 8.22b, 8.23b present gaps in distribution of slip moments inside the genuine (T_{ig}) period of forcing (returned from the value of absolute maximum of the gap width $dF(j,i)^{abs}_{\max}$, here 0.0332327 s), which is divided into 1000 intervals.

From the analysis of the gap spectra we can conclude that synchronization is present at the forcing frequency of 30 Hz and the genuine forcing period $T_{ig} = 1/\mathrm{f} = 0.0332327$ can be extracted with no less than 0.01 Hz accuracy. It is evident that the forcing frequency can be determined accurately from the observed synchronized slip recurrence spectra.

The above approach has been tested on the Catalogue of Caucasian earthquakes of M. Nodia Institute of Geophysics and some significant gaps related to tidal effects were revealed (Chapter 18).

We hope that the methods applied in the present work to the laboratory data can be used in future for detection and quantitative assessment of seismic process synchronization strength induced by a weak external impact, such as tides, reservoir loading, etc (Heaton, 1975; Nikolaev V. 2003; Grasso, 1998).

8.7 Phase Time Delay

The acoustic response lags behind the periodic forcing phase; the lag is inversely proportional to the forcing intensity (Fig. 8.24a, b, c, d). The delay is quite similar for both AE burst onsets and AE wave train maxima. The dependence of phase delay on the intensity of periodic or pulse-like forcing points to a nonlinear response of the system to a weak external impact.

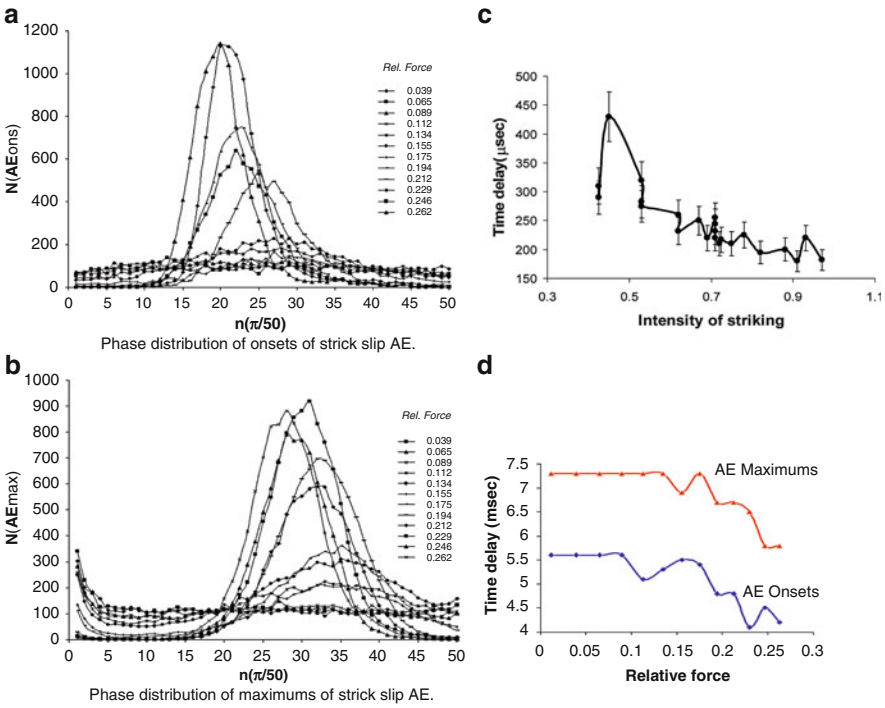

Fig. 8.24 AE phase delay relative to forcing phase: distributions of AE number versus delays for: (**a**) onsets and (**b**) maximums of acoustic signal at periodic EM forcing. (**c**) Time delays for slips triggered by mechanical strike. (**d**) Phase time delays at synchronization by periodic EM forcing for panels a and b

8.8 Synchronization by Mechanical Forcing

Of course, synchronization of stick-slip can be achieved by a weak mechanical forcing also. Such experiments are quite numerous as the phenomenon of stick-slip is ubiquitous in friction processes and it is considered as a negative factor, disturbing the stable displacement of contacting surfaces. In order to achieve smooth functioning of technical systems with friction, application of weak mechanical vibrations of relatively high frequency is studied mainly as a tool for stabilization of friction process (Bureau et al., 2000; Perfettini et al., 2001; Boissou et al., 1998). It has been found that at some intensity of mechanical forcing (but still much less than the main driving force) the stick-slip phenomenon is strongly reduced. At the same time, it is clear from analysis of recordings (Fig. 8.25) that what is considered as stabilization of friction is in fact the stick-slip of small amplitude synchronized with the (high) frequency of forcing. Thus, the stabilization of motion is achieved not by elimination of stick-slip, but by drastic decrease of amplitude of slips, which occur much more frequently than in motion without forcing.

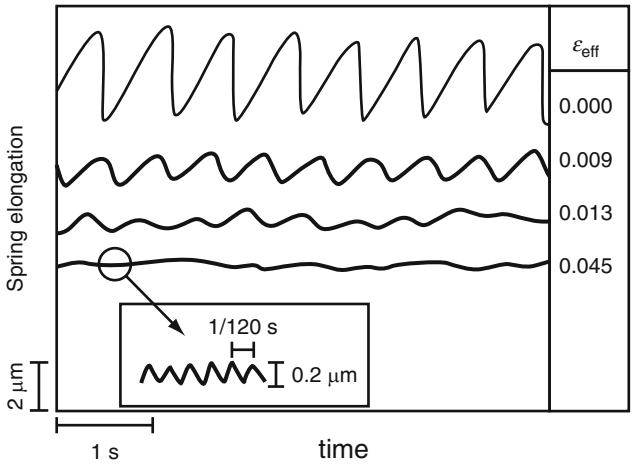

Fig. 8.25 Time evolution of the loading spring elongation for $v = 8$ μm/s and different modulation amplitudes ε_{eff} indicated at the right end of each trace. The bifurcation sequence from stick-slip to stable sliding is evident. The insert is a blow-up of the stable sliding trace showing the remaining oscillating response at the frequency of the load modulation $f = 120$ Hz, much higher than the stick-slip frequency (Bureau, 2000). It seems that what is considered as stabilization is indeed a synchronization of slips with quantization of slip amplitudes

The phenomenon can be considered as a "quantization" of slips, which has been observed also in our experiments with EM forcing (Fig. 8.15). Thus, a single dynamic instability (slip) of magnitude of the order of 3.5 μm in a non-modified friction process is released in the same time interval by 12 small-scale events of magnitude 0.2 μm in synchronized friction as result of quantization. In total, the cumulative slip rate of 12 small displacements was 2.4 μm/s, which is close to the one large slip rate of 3.5 μm/s.

It is unrealistic at present, but the quantization effect of periodic forcing can in principle be considered as a tool for reducing the magnitude of impending strong earthquake.

8.9 High Order Synchronization of Stick-Slip Process: Experiments on Spring-Slider System

In the previous chapters we considered relatively simple synchronization regimes. At the same time it is well known that when the processes of various timescales are coupled, there is a possibility of high order synchronization (HOS). Namely, if ω_n is the natural frequency of first (driven) oscillator, ω is that of the second (forcing) one and Ω is the resulting frequency of driven system under forcing, the system tends to synchronize at different integer ratios of ω/Ω. Such effects are observed, for

example, in biological systems, lasers, electronic relaxation generators, etc (Pikovsky et al., 2003; Kantz, Schreiber, 1997).

Our experiments were aimed to reveal HOS in the frictional system, namely in the stick-slip process of spring-slider setup, subjected to weak electromagnetic (EM) or mechanical forcing.

8.9.1 High Order Synchronization

In the paper the following definitions are used: ω_0 – natural frequency of autonomous oscillator (here spring-slider system); T_0 – corresponding natural period; and ω, T, and ϕ — forcing frequency, period and phase, respectively; Ω, T_{obs}, and ϕ_{obs} – frequency, period and phase, respectively, of autonomous oscillator observed after application of forcing.

There are several kinds of synchronization between oscillating system with natural frequency ω_0 and forcing frequency $\omega = 2\pi f$. We are looking for the phase synchronization (PS), when amplitudes are irregular and uncorrelated, but the frequencies ω and Ω are adjusted, i.e., there is a regular phase shift between ω and Ω.

High-order or (*n:m)* synchronization means that the observed and forcing frequencies satisfy the equation (Pikovsky et al. 2003):

$$n\ \omega = m, \quad \text{or} \quad nT_{obs} = mT_f, \tag{8.14}$$

where n and m are some integer numbers. In our case, ω is the EM or mechanical forcing frequency and Ω is the observed frequency of AE bursts under forcing. The ratio n/m is called the winding or rotation number ρ and is defined as:

$$\rho = \Omega/\omega = T_f/T_{obs}. \tag{8.15}$$

This condition of so-called high-order synchronization can also be incorporated in the general framework of the frequency-locking model, using equation (8.14) ; in this case the ratio *n:m* is the winding number: $\rho = n/m$. The phase-locking can be also expressed in terms of the oscillators' phases:

$$|n\phi - m\phi_{obs}| < const, \tag{8.16}$$

where ϕ is the phase of the forcing and Ω is that of the kicked oscillator.

8.9.2 HOS Synchronization by Electromagnetic Forcing

Figure 8.12 represents actually the example of high order ($n/m = 1{:}2$) synchronization. The experiment shows that the addition to the high frequency EM signal (40 Hz) of a strong enough component of the constant electric field invokes transition from 1:2 to 1:1 synchronization.

The same 1:1 regime can be obtained also upon application of relatively low frequency ($T_0 = 0.5$ s) signal (see the left part of Fig. 8.26). At still lower forcing frequencies, for example, $T_0 = 4.5$ s, the stick-slip process demonstrates swarm-like behavior: one EM forcing generates dozens of AE bursts (see the right part of Fig. 8.26).

Figure 8.27 represents the HOS of stick-slip at EM forcing by pulses of different duration. Both the onsets of swarms and these of the individual events within sequences (swarms) turn out to be very well organized.

The onsets of swarms have almost the same delay relative to the times of onsets of identical forcing (t_{if0}; $i = 1, 2 \ldots . k$, where i is the number of forcing pulse) and the events within swarms manifest regular phase difference. Besides, even small difference in the duration of the forcing pulses causes regular changes in the delays, number of AE bursts in the induced swarm and in phase differences. Characteristics of EM forcing and AE response are as follows. Short forcing pulses: $n{:}m = 1/3$; mean duration $t = 0.618$ s; mean delay $t_{if0} = 0.295$ s; the AE response consists of three consecutive bursts with mean phase differences of 0.258; 0.411; 0.537 s, and St. Dev. of 0.037; 0.048; 0.034, respectively. Long forcing pulses: $n{:}m = 1/4$ or $1/5$; mean duration $t = 0.82$ s; mean delay $t_{if0} = 0.358$ s; the AE response consists of four

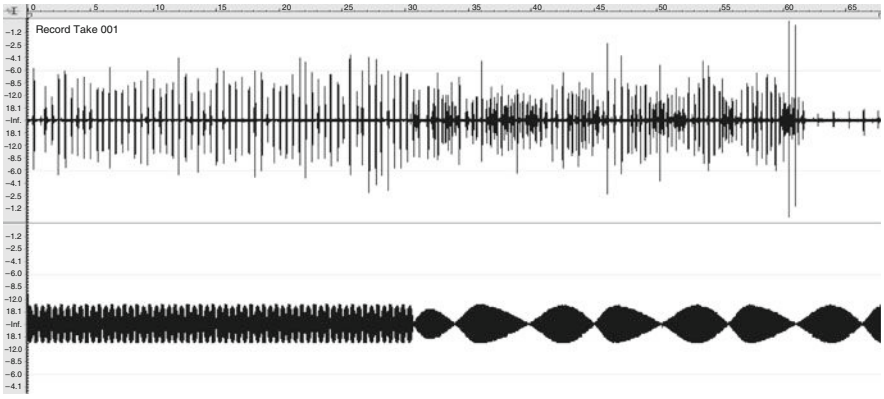

Fig. 8.26 Transition (bifurcation) in stick-slip from 1:1 synchronization to high order synchronization at increasing period of forcing from 0.5 s to 4.5 s (exp: Zura5). Note that in Figs. 8.26, 8.27a and 8.28a the forcing signal was filled by high frequency (HF) oscillations in order to visualize the low frequency forcing on the computer screen; the HF signal was applied only to computer and not to the rock plates

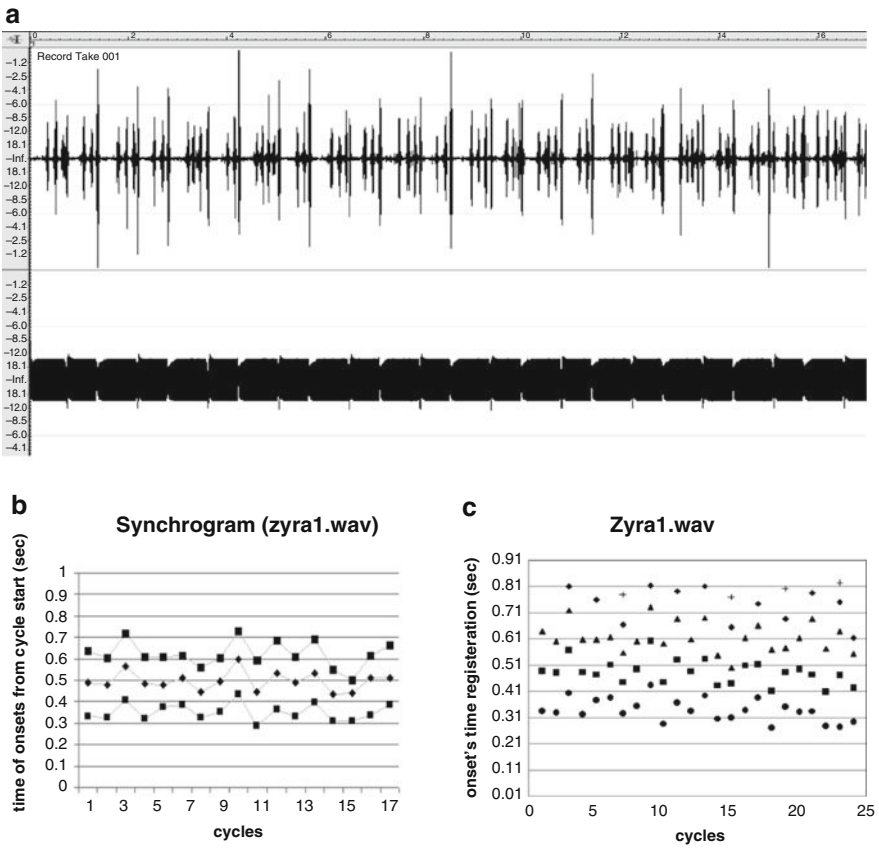

Fig. 8.27 High order synchronization: $n<m$ (exp. Zyra1). Note that the onsets of swarms and those of the individual events within sequences (swarms) turn out to be very well organized (see text). (**a**) High order synchronization: $n<m$; (**b**) synchrogram for short forcing pulses $n:m = 1/3$; (**c**) synchrogram for longer forcing pulses $n:m = 1/4$ or $1/5$. Note that the onsets of swarms and those of the individual events within sequences (swarms) turn out to be very well organized (see text)

consecutive pulses with mean phase differences of 0.268; 0.467; 0.601; 0.736, and St.Dev. of 0.046; 0.05; 0.07; 0.055; 0.046, respectively.

Figure 8.28 presents even more numerous AE swarms generated by longer EM pulses; in this case the swarms contain up to 40 AE events, so $n:m \approx 1/40$. Again, the AE bursts within the swarm are well organized. The first ten of bursts show almost constant phase shift relative to the EM forcing onsets. The following bursts demonstrate a regular small increase of the phase delay in sequential swarms.

So, it seems that the lower the frequency of forcing, the larger the number of triggered synchronized events in the forcing-generated AE swarms. Probably the same mechanism can lead to formation of seismic swarms.

Besides $n<m$ coupling, we observe also $n>m$ HOS (Fig. 8.29 a, b). Here the AE bursts occur rarely in comparison with EM forcing pulses. The forcing pulse

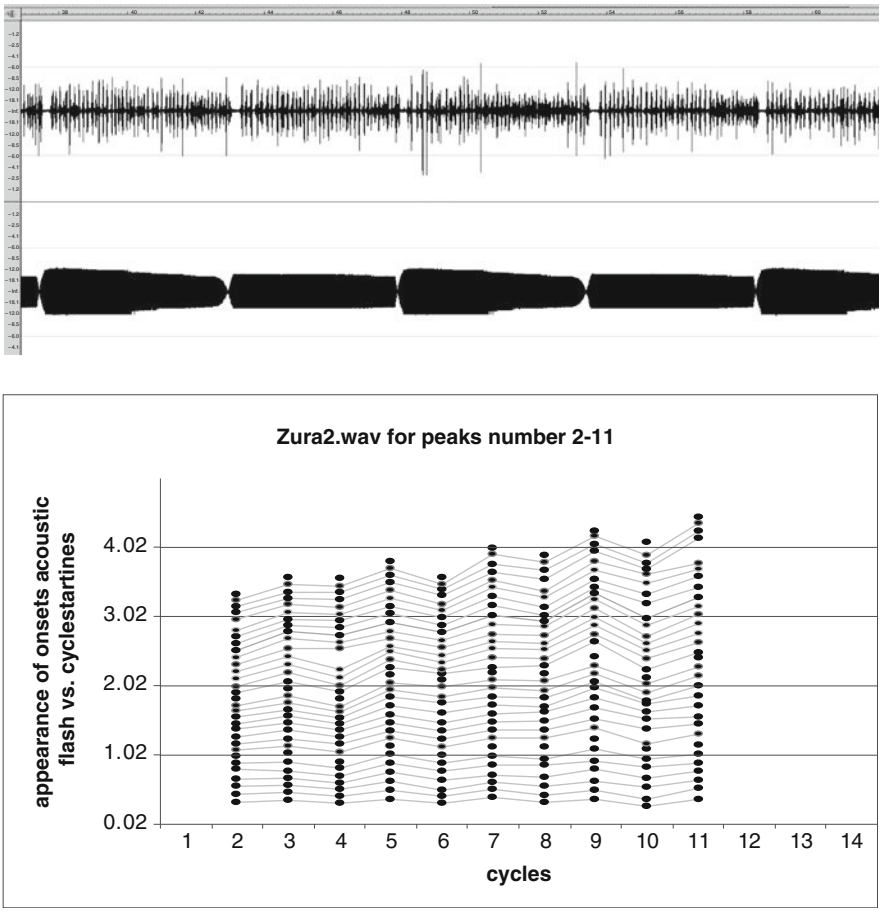

Fig. 8.28 High order synchronization: $n{:}m \approx 1/40$ (exp. Zura2); a) wav. file; b) stroboscopic diagram (synchrogram) for the first 31 AE bursts in the swarms number 2-11 generated by 11 forcing EM pulses; note the stripe structure of synchrogram, which shows that the phase shift between EM forcing and AE pulses is almost constant for the first 10 slips

(repetition) rate was $T_f = 1.8$ sec, AE delay relative to the pulse onset – 0.24 s. The observed AE period was $T_{obs} = 25$ s. Thus, in this case $n>m$, namely the winding number is 14:1. Fig. 8.29 b presents the AE distribution relative to the forcing period phase, which is very sharp though slips wait quite long (hundreds of forcing periods) to occur.

8.9.3 HOS by Mechanical Forcing

We also investigated synchronization of the same spring-slider system under weak periodic mechanical forcing (Chelidze et al., 2007; Varamashvili et al., 2008). The

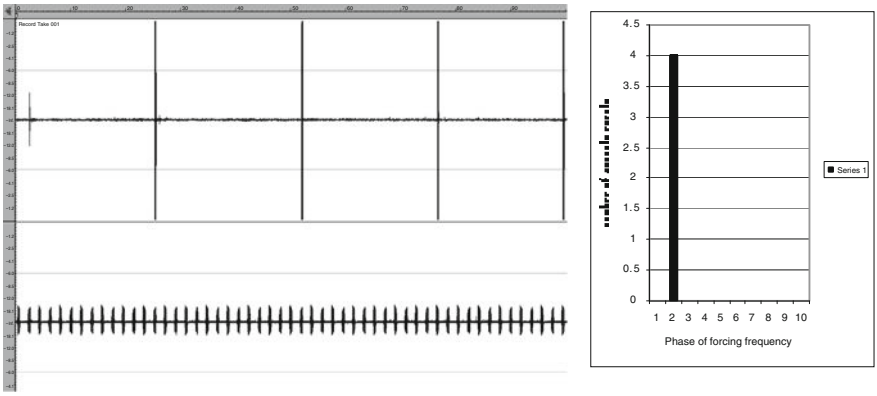

Fig. 8.29 High order EM synchronization: $n>m$; (exp.Sopo1). $T_f = 1.815$ s; delay time = 0.240 ms; $T_{ob} = 25$ s; $n\ \omega = m\ \Omega$; $14n \cong m$. (a) recording of AE at synchronization by EM pulses; (b). histogram of AE bursts distribution in phases of EM forcing

experiments were conducted for two modes of mechanical forcing: (i) the forcing is applied normal to the slip surface and (ii) forcing is applied parallel to the slip surface; for brevity we will refer to them as normal and tangential forcing, respectively. In the case of normally directed forcing we calculated the maximum value of mechanical forcing, which corresponds to the maximum measured voltage applied to mechanical vibrator (i.e., when the voltage applied to the vibrator equals 6.5 V). The mass of the oscillating element of the vibrator m is $\approx$ 20 g, so we obtain for oscillating element of the vibrator the natural frequency f: $f = \sqrt{k/m} = 5$ Hz, where k is the stiffness of the vibrator spring. Then $k = 25\ m = 0.5$ N/m.

The maximum deflection x_{max} of the oscillating element at the applied voltage 6.5 V equals $x_{max} \approx 4.10^{-3}m$, so the corresponding (maximal) intensity of forcing F_{max} is $F_{\max} = kx_{\max} \approx 2.10^{-3}$N.

At smaller voltages, the forcing is much weaker – our assessment for 1V is $\sim 5.10^{-4}N$. Thus, the forcing was always much less than the driving force $F = 4\ N$. Similar numbers were obtained for tangential mechanical forcing. The forcing frequencies were 30 Hz for the tangential and 20 Hz for the normal loading cases. In both cases, the forcing rate was larger than the dragging rate, which means that the synchronization of the process is possible.

Figure 8.30 a, b presents experimental records, when the mechanical forcing is in the range $(5.10^{-5} - 2.10^{-3})$ N, which corresponds to 4 V voltage applied to the vibrator.

Distributions of the AE burst onsets relative to the phase (in decimals) of mechanical forcing period for the normal forcing are presented in Fig. 8.31.

At low voltages (up to 1V) the onsets are more or less randomly distributed in the decimals of the forcing period. Voltage increase results in concentration of the offsets at a definite part of forcing period, namely in the first and the last decimals of forcing phase. Evidently, increasing of voltage applied to mechanical vibrator

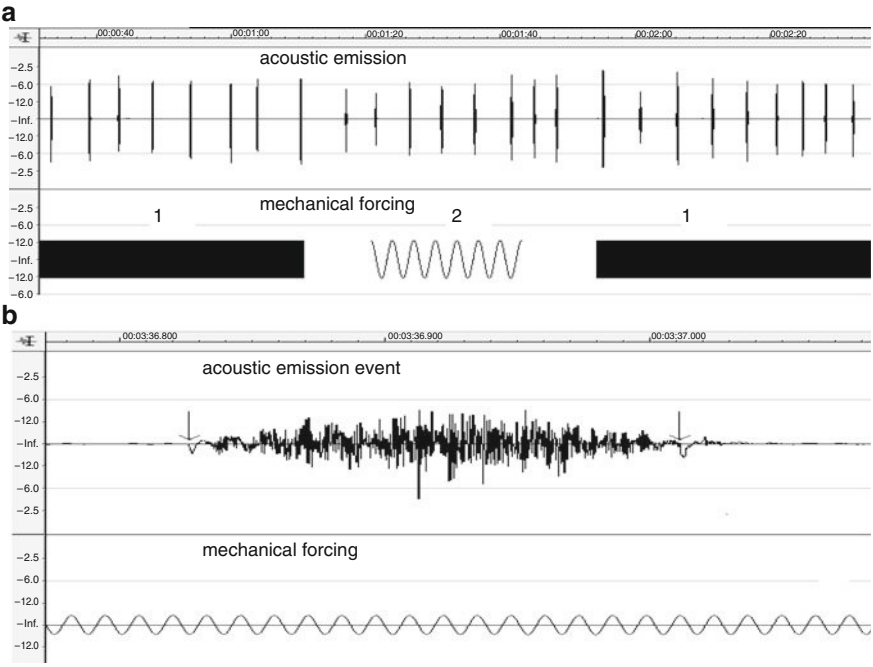

Fig. 8.30 (**a**) The full record of AE bursts (upper channel) and mechanical forcing (lower channel), sections 1 — total record of forcing, corresponding to the time scale, shown at the upper side of figure; section 2 — part of forcing record in the expanded form; here the time scale is disregarded in order to visualize the form of forcing signal during synchronized stick-slip. Mechanical forcing corresponds to vibration intensity generated by application of 4 V voltage to the vibrator; (**b**) A single acoustic pulse and corresponding tangential mechanical forcing on the expanded scale. The initial slow deviation from the background line is considered as the onset of the AE pulse and the start of slow terminal phase as a pulse termination; these moments are marked by arrows

promotes synchronization of AE offsets with external forcing. The same behavior is observed for tangential mechanical forcing (Fig. 8.32).

Thus at low voltages (up to 2 V) the onsets are more or less randomly distributed in the decimals of the forcing period (Figs. 8.31, 8.32). Voltage increase results in concentration of the offsets at a definite part of forcing period, namely in the first and the last decimals of forcing period for normal forcing; in the case of tangential forcing (Fig. 8.32) synchronization is most pronounced in the interval 0.25–0.5 of the forcing period and fills the gap observed for normal forcing (Fig. 8.31).

Alteration of the forcing frequency affects the phase distribution of AE. Figure 8.33 (the left column) shows the AE distribution for tangential forcing at frequency 80 Hz. It is evident that the maximum of AE shifts to other phases of forcing period compared to the distribution for 20 Hz.

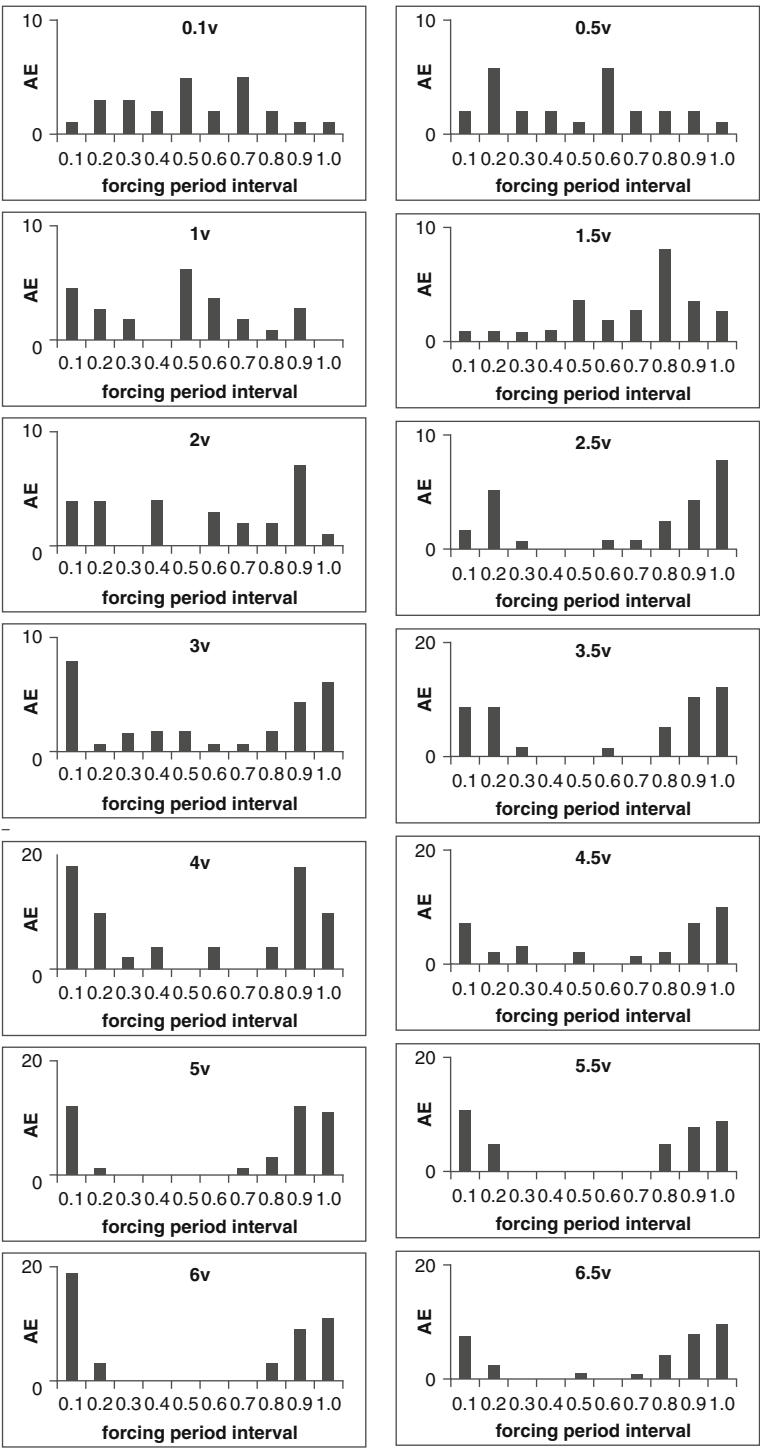

Fig. 8.31 Distribution of acoustic emission onsets relative to mechanical forcing period phases (in decimals) for different intensities of normal forcing. Forcing frequency – 20 Hz

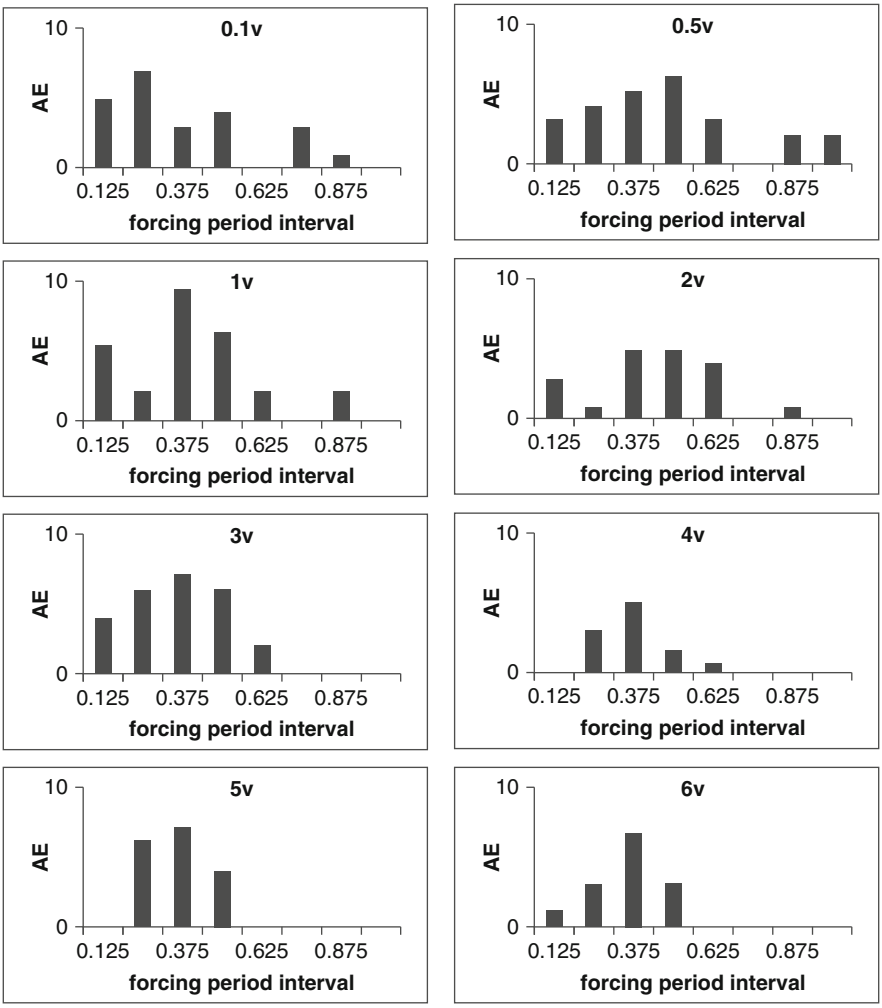

Fig. 8.32 Distribution of acoustic emission onsets number relative to the forcing period phase (in decimals) for different intensities of tangential forcing. Forcing frequency – 30 Hz

8.9.4 Synchronization of AE Signal Terminations

It was a surprise to discover that not only AE onsets can be synchronized by a weak mechanical forcing; Fig. 8.33 (right column) illustrates that the terminal parts of the signal also are synchronized by forcing with the same strength as the onsets.

We suppose that the forcing (here 80 Hz) can affect not only the phases of onsets but also the phases of terminations of AE bursts, but their influence is realized in quite different phases of forcing: presumably, the onsets are triggered by tangential

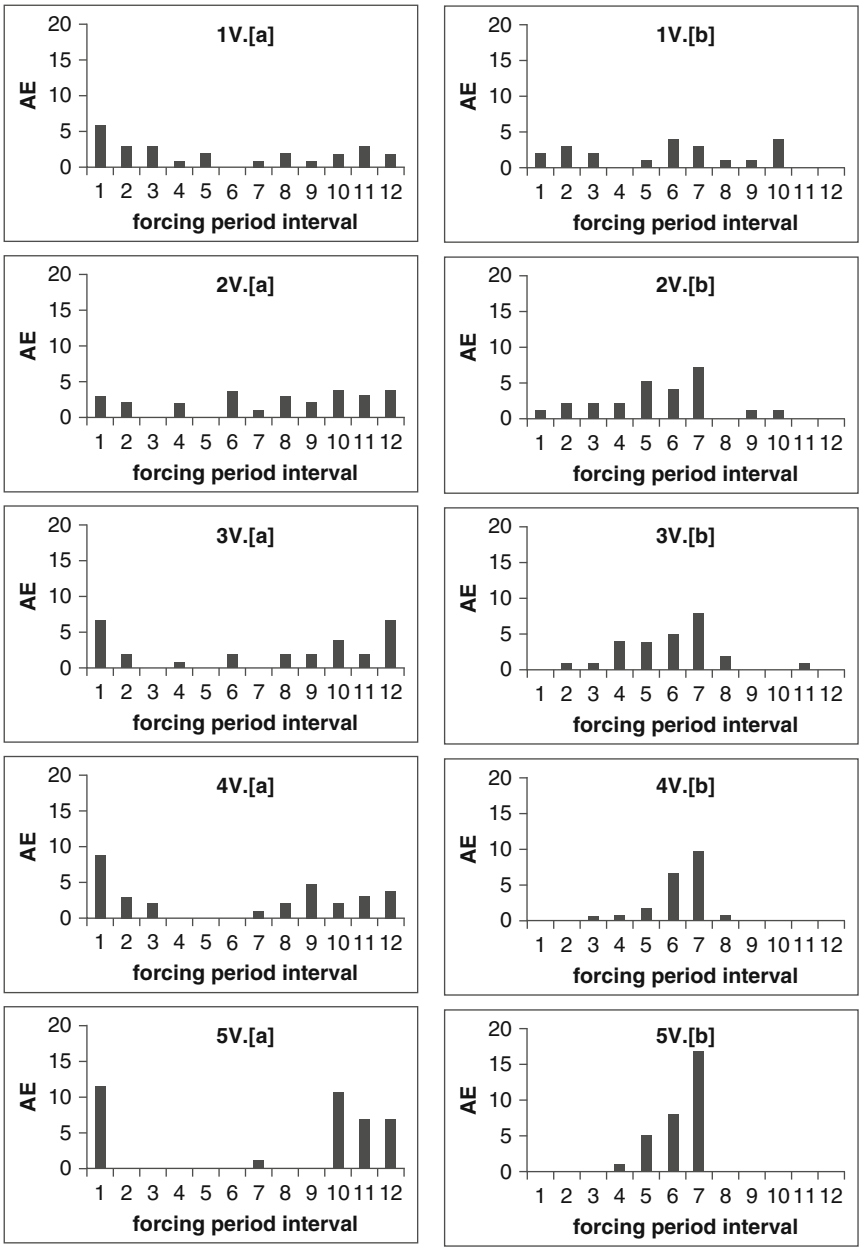

Fig. 8.33 Distribution of acoustic emission onsets (the left column) and terminations (the right column) relative to the (mechanical) forcing period phase (in twelfths of the forcing period) for different intensities of tangential forcing. Forcing frequency – 80 Hz

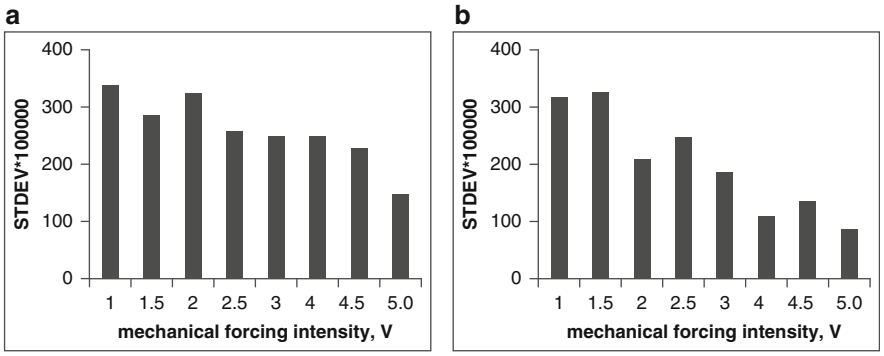

Fig. 8.34 Standard deviation of onsets (**a**) and terminations (**b**) distributions for different intensities of external applied voltages, which are proportional to intensity of (tangential) mechanical forcing

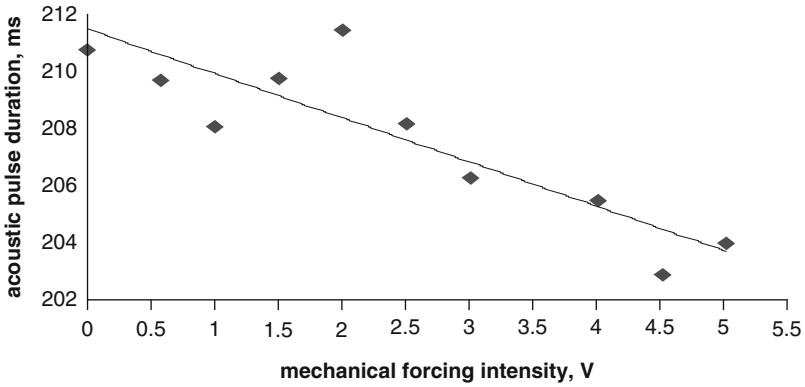

Fig. 8.35 Mean duration of stick-slip generated acoustic pulses for different intensity of normal mechanical forcing, with a trend line

forcing around the minimum area of forcing period and suppressed by forcing in the maximum area of forcing period.

The standard deviation of onset and termination times regularly decreases with increase of forcing intensity (Fig. 8.34).

Besides better synchronization of onsets and terminations, the increase in forcing intensity also brings on regular shortening of duration of AE bursts (Fig. 8.35).

It is evident that increasing voltage applied to the vibrator promotes synchronization of AE offsets with external forcing.

It is striking that the AE bursts are well synchronized though the waiting interval of bursts varies between 100-200 periods of forcing, i.e., to initiate the phase-synchronized slip event the forcing oscillator should pump the energy of hundreds of oscillations to the slider-spring system.

The important conclusion for the much discussed interaction between tidal deformation and EQ-s (Beeler, Lockner, 2003; Scholz, 2003) is that in order to

find it we should not only look for direct 1:1 correlation between events recurrence frequency and forcing, namely for the increase of seismicity exactly at the tide frequency (say, 12 h). The high order phase synchronization can occur at multiples of tide frequency like it was shown in laboratory experiments. It is important to note that HOS can be responsible for phase synchronization of AE or seismic events irrelative to the duration of their nucleation; of course, the optimal condition of synchronization (minimal forcing) should correspond to the forcing period, close to natural event nucleation time. Additional complication arises from the phenomenon of delay; the response can be shifted quite significantly for weak forcing. Thus, the question of tidal forcing of earthquakes should be reconsidered taking into account new experimental evidence.

8.10 EM Synchronization: Physical Mechanism of Period Doubling

It is well known that the slider-spring system displays the stick-slip behavior described by the nonlinear equations (Dietrich, 1979; Ruina, 1983; Rice et al., 2001; Becker, 2000): $\tau = \sigma_n[\mu_0 + \Theta + A\ln(v_d/v_c)]$; $\dot{\Theta} = (-v_d/d_c)[\Theta + B\ln(v_d/v_c)]$, where τ is the friction stress, σ_n is the normal stress, Θ is the surface state parameter, μ_0 is a nominal (constant) value of friction, d_c is the dimension of asperity, v_d is the slip speed, v_0 is the initial value of v_d and A and B are constants. Both theoretical solutions and experiments demonstrate a possibility of very different behavior of the system depending on the conditions of the test. For example, nonlinear analysis of a simple quasi-static slider-spring system with rate- and state-dependent friction shows chaotic dynamics behavior in the deterministic sense (Becker, 2000). In particular, at the critical value of spring stiffness, the friction stress may undergo oscillations close to periodical.

On the other hand, it has been shown (Ott et al., 1990; Bocaletti et al., 2000) that it is possible to control the behavior of chaotic systems using very small feedback impact. The matter is that the attractor of a chaotic system contains an infinite number of unstable periodic orbits. Given such an attractor, one can choose some of the low-period orbits (or steady states) embedded in the attractor and use a feedback perturbation of an accessible parameter P of the system in order to stabilize the chosen orbit and thus improve the performance of the system, for example, convert the chaotic behavior into periodic process. The extreme sensitivity of chaotic systems to external impact allows to control the dynamic state of the physical object by using a very small perturbation. Experimental control of chaos has been successfully realized first by Ditto et al. (1990) on the parametrically driven magnetoelastic ribbon and then by many others on mechanical, electronic, biological and chemical systems (see Ott et al., 1994).

An alternative mathematical formalism for explanation of control phenomenon is provided by synchronization theory (Blekhman, 1988; Lursmanashvili et al., 2001;

Pikovsky et al., 2003). The crux of this approach is the existence of some critical parameter in the system that causes its relaxation. Then small periodic impact can synchronize relaxation of the whole system with the period of impact, if some force regularly drives the system close to the critical state. Let us consider some relaxation process in which the intensity U_r (it can be related to voltage, stress, etc) builds up slowly to some critical value U_c; when $U_r = U_c$, the intensity drops instantly to some initial value. Then the application of synchronizing pulses of relatively small amplitude U_s and of very short duration may impose coherency of these drops with the timing of pulses, as now the condition of criticality is $U_r + U_s = U_c$ or, in the case of sinusoidal impact, $U_r + a\sin(\omega t + \varphi) = U_c$, where ω, a and φ are the angular frequency, phase and amplitude of periodic impact, respectively. This means that intensity drops occur, when the increasing value of U_r is equal to $U_c - a\sin(\omega t + \phi)$; for details see Chapter 18. It has been shown (Blekhman, 1988; Pikovsky et al., 2003) that synchronization may appear at even weak coupling between objects with significantly different characteristic frequencies that implies nonlinear interaction of objects.

What is the physical mechanism leading to synchronization? In case of mechanical excitation, synchronization is connected with mechanical triggering of microslips in the system that is close to critical state and thus reveals sensitive dependence on (small) external perturbation.

In the case of EM forcing, the driving mechanism of triggering is electrostriction (equations 8.5 and 8.6); synchronization occurs when the oscillating EM component of Coulomb stress is strong enough.

We suppose that EM synchronization is connected with polarization of surfaces of fixed and sliding samples. As the polarization forces arise at both polarities of applied periodic field, it seems reasonable to expect that the synchronization follows each reversal of EM field. As the mechanical instabilities synchronize with both positive and negative sections of sinusoid (the response is symmetric) we can postulate that the additional elastic strain, u, induced by forcing has a quadratic dependence on the intensity of electrical field $E = E_m \sin \omega t$:

$$u = kE^2 \tag{8.17}$$

which is the well known expression of electrostriction in solids (compare with expressions 8.3 and 8.4); here k is some proportionality constant depending on the forcing frequency and physical properties of rock (Chernyak, 1978).

If the electromagnetic forcing contains, besides the periodic component, also a constant one, that is:

$$E = E_c + E_m \sin \omega t, \tag{8.18}$$

then, after inserting (8.18) into (8.17), the elastic response becomes:

$$u = kl(E_m)^2 \left\{ 1 + 2(E_c/E_m)^2 + 4(E_c/E_m) \sin \omega t - \cos 2\omega t \right\}, \tag{8.19}$$

where $k1$ is proportionality constant, which depends on the forcing frequency, physical properties of rock and constant component intensity E_c. It is evident that the stick-slip response to forcing in the latter case depends on the value of ratio E_c/E_m. At $E_c/E_m << 1$ the $\cos 2\omega t$ term of (19) is dominant, which means that the slip events will occur with the double frequency of forcing, but at $E_c/E_m >> 1$ the slip regime is governed by the $\sin \omega t$ term, that is, only one slip event occurs per period of forcing. These conclusions are confirmed by experiments (Fig. 8.12).

8.11 Conclusions

The phase synchronization of stick-slip process induced by a weak electromagnetic or mechanical periodic forcing was analyzed. Stick-slip events were identified as acoustic emission (AE) bursts and recorded on the sound card of computer. The onsets of acoustic events were picked by special program using Akaike criterion. For quantitative measuring of synchronization strength, several modern tools of nonlinear dynamics were used (mean effective phase diffusion coefficient, Shannon entropy based characteristic phase synchronization measure *(γH-Sh)*, recurrence plots, and recurrence quantitative analysis RQA, namely, percent of determinism %DET, etc).

An application of varying frequencies and intensities of forcing allows to compile Arnold's tongue for EM forcing. We found that not only the onsets/maxima of a definite kind of AE signals are synchronized with forcing, but also AE wave train terminations.

The effect of high order synchronization of stick-slip events by weak electromagnetic or mechanical periodic forcing was discovered. There were two kinds of high order synchronization: (i) one or more AE bursts during one forcing period and (ii) one AE burst during many forcing periods.

It was found that the onset time of the synchronized slip events lags behind the forcing phase; the delay is smaller for stronger forcing.

The results obtained point to possibility of revealing some new fine details in the stick-slip process which can be very useful for refining the physical mechanism of frictional motion in general. These findings can also help to find new regularities in seismic time series.

Acknowledgements The authors express their gratitude to the Georgian National Science Foundation (Grant No GNSF/ST06/5-028) and INTAS foundation (Ref. *N* 05-100008-7889) for financial support.

References

Akay, A. 2002, Acoustics of Friction. J. Acoust. Soc. Am., **111**, 1525–1548.

Bak, P., C. Tang and K. Wiesenfeld. 1988. Self-organized criticality. Phys. Rev. A38, 364–374.

Becker, T.W. 2000. Deterministic Chaos in the Two State-variable Friction Sliders and the Effect of Elastic Interactions. In: Rundle, J.B, Turcotte, D.L. and Klein, W. (Eds.), Geocomplexity and the Physics of Earthquakes. American Geophysical Union, Washington, DC, pp.5–26.

Ben-Zion, Y., Collective Behavior of Earthquakes and Faults: Continuum-Discrete Transitions, Evolutionary Changes and Corresponding Dynamic Regimes, Rev. Geophysics, **46**, RG4006, doi:10.1029/2008RG000260, 2008.

Beeler, N.M. and D.A. Lockner. 2003. Why earthquakes correlate weakly with the solid Earth tides: Effects of periodic stress on the rate and probability of earthquake occurrence. Journal of Geophysical Research, **B108**, 2391–2405.

Benguigi, L. (1988). Simulation of dielectric failure by means of resistor-diode random lattices. Phys. Rev. B 38, 7211–7214.

Blekhman I.I., 1988. Synchronization in Science and Technology. ASME Press, New York.

Brace W. E., and I.D. Byerlee. 1966. Stick slip as a mechanism for earthquakes. Science, **153**, 990–992.

Bocaletti, S., Grebogi, C., Lay, Y.-C., Manchini, H., Maza, D. 2000. The Control of Chaos: Theory and Applications. Physics Reports. 329, 103–197.

Bouissou, S., Petit, J., Barquins, M. 1998. Experimental evidence of contact loss during stick-slip: possible implications for seismic behavior. Tectonophysics, **295**, 341–350.

Bureau, L., T. Baumberger and C. Caroli, 2000, Shear response of a frictional influence to a normal load modulation. Phys. Rev. E, **62**, 6810–6820.

Chelidze, T., N. Varamashvili, M. Devidze, Z. Chelidze, V. Chikhladze and T. Matcharashvili. 2002. Laboratory study of electromagnetic initiation of slip. Annals of Geophysics, **45**, 587–599

Chelidze, T., Lursmanashvili, O. 2003. Electromagnetic and mechanical control of slip: laboratory experiments with slider system. Nonlinear Processes in Geophysics, 20, 1–8.

Chelidze, T., T. Matcharashvili. 2003a. Electromagnetic control of earthquake dynamics? Computers&Geosciences, 29, 587–593.

Chelidze, T., A. Gvelesiani, N. Varamashvili, M. Devidze, V. Chikchladze, Z. Chelidze and M. Elashvili. 2004b. Electromagnetic initiation of slip: laboratory model. Acta Geophysica Polonica, **52**, 49–62

Chelidze, T., T. Matcharashvili, J. Gogiashvili, O. Lursmanashvili and M. Devidze. 2005. Phase synchronization of slip in laboratory slider system. Nonlinear Processes in Geophysics, **12**, 1–8

Chelidze, T., O. Lursmanashvili, T. Matcharashvili and M. Devidze. 2006. Triggering and synchronization of stick slip: waiting times and frequency-energy distribution Tectonophysics, **424**, 139–155

Chelidze T., and T. Matcharashvili. 2007. Complexity of seismic process, measuring and applications – A review, Tectonophysics, **431**, 49–61.

Chelidze, T. Matcharashvili, O. Lursmanashvili, N. Varamashvili. 2008. Acoustics of stick-slip deformation under external forcing: the model of seismic process synchronization. In: Advanced Topics in Geology and Seismology. D. Triantis, M. Jelenska, F. Vallianatos (Eds). University of Cambridge, WSEAS Press. pp:36–43.

T. Chelidze, O. Lursmanashvili, T. Matcharashvili, N.Varamashvili N. Zhukova, E. Mepharidze. 2009. High order synchronization of stick-slip process: experiments on spring-slider system. Nonlinear Dynamics, DOI 10.1007/s11071-009-9536-6

Chernyak, G. 1978. On the physical nature of seismoelectric effect in rocks. Izvestia Ac. Sci. USSR, Physics of Earth. N2, 108–112, (in Russian).

Dieterich, J.H. 1979. Modeling of rock friction 1. Experimental results and constitutive equations. Journal of Geophysical Research, **84B**, 2161–2168.

Ditto, W.L., Rauseo, S.N. and Spano, M.L. 1990. Experimental control of chaos. Phys. Rev. Lett., 65, 3211–3214.

Grasso, J-R and D. Sornette. 1998 Testing self-organized criticality by induced seismicity. Jour. Geoph.Res., 103, 29 965–29 987.

Heaton T. H. 1975. Tidal Triggering of earthquakes. Geoph.J. of the Royal Astr. Soc., 43, p. 307–326.

Kanamori, H., and E.E. Brodsky. 2004. The physics of earthquakes. Rep. Prog. Phys., **67**, 1429–1496.

Kantz, H., Schreiber T., 1997. Nonlinear time series analysis. Cambridge University Press, Cambridge.

Kurz, J., CU. Grosse, HW Reinhardtet. 2005. Strategies for reliable automatic onset time picking of acoustic emissions and of ultrasound signals in concrete, Ultrasonics, 43, 538–546

Lursmanashvili O. 2001. Role of exogenous factors in initiation of Caucasus Earthquakes Journal of the Georgian Geophysical Society, Issue (A), Physics of Solid Earth, v. 6, pp. 22–27.

Maeda, 1985. A method for reading and checking phase times in autoprocessing system of seismic wave data, J. Seismology Soc. Japan. 38, 365–379.

Marwan, M. 2003.Encounters with neighborhood, Ph.D Thesis.

Nikolaev, A.V. (Ed.). 1994. Induced Seismicity. Moscow, "Nauka", 220 p, (in Russian).

Nikolaev, V. A. 2003. Research of lithospheric stress state on the base of correlation of tidal forces and seismicity. Anakharsys, Moscow (in Russian).

Ott, E., Grebogi, C., Yorke, J.A. 1990. Controlling chaos. Phys.Rev.Lett., 64, 1196–1199.

Perfettini H., J. Schmittbuhl and J.R. Rice. 2001. Frictional response induced by time-dependent fluctuations of the normal loading. Journal of Geophysical Research, **106B**, 13455–13472

Pikovsky, A., Rosenblum, M.G., Kurths. J. 2003. Synchronization: Universal Concept in Nonlinear Science. Cambridge University Press, Cambridge.

Rice J. R., N. Lapusta and K. Ranjith. 2001. Rate and state dependent friction and the stability sliding between elastically deformable solids. Journal of the Mechanics and Physics of Solids, **49**, 1865–1898

Rosenblum, M.G., Pikovsky, A., Kurths. J. 1996. Phase synchronization of chaotic oscillators. Phys. Rev. Lett., 76, 1804–1808.

Rosenblum, M.G., Pikovsky, A., Kurths. J. 1997. Effect of phase synchronization in driven chaotic oscillators. IEEE Trans. CAS-I, 44. 874–881.

Ruina A. 1983. Slip instability and state variable friction laws. Journal of Geophysical Research, **88B**, 10359–10370

Quiroga, R., R Quian Quiroga, A Kraskov, T Kreuz, P Grassberger. 2002. Performance of different synchronization measures in real data, Phys.rev.E, **65**, 041903.

Scholz, C. (1990): The mechanics of earthquakes and faulting (Cambridge Univ. Press. Cambridge.1990)

Sobolev, G., A. Ponomarev, A.Avagimov, V. Zeigarnik. (2000): Initiating acoustic emission with electric actions. In Reports of ESC conference, Madrid.

Sobolev, G.A. and Ponomarev, A.V., 2003. Physics of Earthquakes and Precursors. Moscow, "Nauka", (in Russian).

Scholz C. H. 1998. Earthquakes and friction laws. Nature, **391**, 37–42

Scholz, C.H. 2003. Mechanics of Earthquakes and Faulting. Cambridge University Press, Cambridge.

Sibson R. 1994. Crustal stress, faulting and fluid flow. In: Deformation and Fluid Flow Geological Society, London, Special Publications; 1994; v. 78; p. 69–84

Tamm, I. 1956. Fundamentals of theory of electricity. Moscow (in Russian).

Tarasov, N., H. Tarasova, A. Avagimov and V. Zeigarnik (1999), The effect of high-power electromagnetic pulses on the seismicity of Central Asia and Kazakhstan. Volcanology and Seismology (Moscow), N4-5, 152–160 (in Russian).

Varamashvili, N., T. Chelidze, O. Lursmanashvili. 2008. Phase synchronization of slips by periodical (tangential and normal) mechanical forcing in the spring-slider model. Acta Geophysica, 56, 357–371.

Zbilut, J.P., Webber, C.L. Jr., 1992, Embeddings and delays as derived from quantification of recurrence plots. Physics Letters A, 171, 199–203